Check for updates

JGR Oceans

RESEARCH ARTICLE
10.1029/2021JC017863

Physical Drivers of Biogeochemical Variability in the Polar Front Meander

Xiang Yang[1,2,3], Peter G. Strutton[1,2], Ajitha Cyriac[1], Helen E. Phillips[1,4,5], Nicholas A. Pittman[1,2], and Clara R. Vives[1,2]

[1]Institute for Marine and Antarctic Studies, University of Tasmania, Hobart, TAS, Australia, [2]Australian Research Council Centre of Excellence for Climate Extremes, University of Tasmania, Hobart, TAS, Australia, [3]College of Oceanic and Atmospheric Sciences, Ocean University of China, Qingdao, China, [4]Australian Antarctic Program Partnership, University of Tasmania, Hobart, TAS, Australia, [5]Australian Centre for Excellence in Antarctic Science, University of Tasmania, Hobart, TAS, Australia

Abstract The Southern Ocean plays a vital role in global ocean circulation, and the Polar Front (PF) is one of its most important physical features. The PF meander south of Tasmania, around 153°E, 55°S, is a very dynamic region which spawns mesoscale eddies, and influences local biogeochemistry and sea-air interaction. By using voyage and ancillary data, we investigated the unusually strong spring bloom in the vicinity of the PF meander in 2018. We infer that the upwelling of deep water at the front and in eddies, brings macronutrients and dissolved iron (dFe) to the surface. Chlorophyll concentration peaked at over 0.6 mg m^{-3}, which is anomalously high for this area. With reduced iron limitation, the physiological characteristics of phytoplankton in the northern, downstream part of the study area also changed. The photochemical efficiency was improved and released this area from its usual high-nutrient low-chlorophyll (HNLC) status. This was mainly indicated by the increase in the dawn Fv/Fm maximum (indictor of photochemical efficiency) from 0.2 to over 0.5. With the biomass increase and healthier community status, we observed consumption of surface dissolved inorganic carbon and increased particulate organic carbon production to about 40 μmol L^{-1}, forming a weak local carbon sink. Through the investigation of multiple years, a weak positive correlation between mixed layer depth shoaling and phytoplankton growth was found, but there was significant interannual variability in this relationship, likely caused by variable eddy conditions and dFe delivery.

Plain Language Summary Eddies are circulating ocean features with a diameter of about 100 km, which last for weeks to months. At any given time, there are about 1,300 eddies in the Southern Ocean. Eddies transport, mix, and stir nutrients (like nitrate, silicate, and dissolved iron) which can influence local biological processes. Using data from a voyage in the Southern Ocean south of Tasmania, we investigated a spring phytoplankton bloom promoted by local physical processes like eddy formation. With the lifting of iron limitation, we found that the biomass here increased rapidly in a short time, and the phytoplankton became healthier. As a result of this, surface dissolved carbon was consumed, and organic carbon production increased. Based on a 20-year retrospective satellite study, a positive relationship between mixed layer depth shoaling and biomass increase was revealed, but strong interannual variability also existed.

Key Points:

- An unusually strong spring bloom was observed in a highly unstable Polar Front meander south of Tasmania
- Physiological characteristics of phytoplankton, measured by fluorescence, identified iron-sufficient and iron-deficient regions
- The strong bloom was likely favored by local and recent mixed layer variability and mesoscale processes, and created a local carbon sink

Supporting Information:

Supporting Information may be found in the online version of this article.

Correspondence to:

X. Yang,
xiang.yang@utas.edu.au

Citation:

Yang, X., Strutton, P. G., Cyriac, A., Phillips, H. E., Pittman, N. A., & Vives, C. R. (2022). Physical drivers of biogeochemical variability in the Polar Front meander. *Journal of Geophysical Research: Oceans*, *127*, e2021JC017863. https://doi.org/10.1029/2021JC017863

Received 4 AUG 2021
Accepted 17 MAY 2022

© 2022. The Authors.
This is an open access article under the terms of the Creative Commons Attribution-NonCommercial-NoDerivs License, which permits use and distribution in any medium, provided the original work is properly cited, the use is non-commercial and no modifications or adaptations are made.

1. Introduction

The oceans play a vital role in regulating climate by taking up over 25% of anthropogenic carbon dioxide (CO_2), while the Southern Ocean south of 40°S is responsible for 40% of total ocean carbon uptake (Le Quéré et al., 2018; Moreau et al., 2017; Rintoul & Naveira Garabato, 2013; Sabine et al., 2004). However, there is interannual to decadal variability in the magnitude of this sink. It weakened between the 1980s to the early 2000s (Le Quéré et al., 2018) and has since recovered (Landschützer et al., 2015). For prediction of future climate, it is important that we understand the mechanisms of carbon cycling and sequestration in this globally significant ocean.

The Antarctic Circumpolar Current (ACC) is a powerful current system that consists of many narrow, coherent jets (Abbott et al., 2001; Sokolov & Rintoul, 2009), and it dominates the large-scale circulation of the Southern Ocean (Talley et al., 2011). Due to this complex circulation system, along with the influence of light and iron on biological activities, the Southern Ocean has remarkable nutrient heterogeneity and is a famously high-nutrient low-chlorophyll (HNLC) area (Garabato et al., 2001; Hoffmann et al., 2008; Janssen et al., 2020;

Lannuzel et al., 2011). Among the ACC fronts, the Polar Front (PF) has been considered the most important for biogeochemistry, because of its strong meridional gradient of macronutrients (Freeman et al., 2019; Garabato et al., 2001; Janssen et al., 2020; Jones et al., 2015) due to the upwelling of high-nutrient Circumpolar Deep Water (CDW) to its south (Talley et al., 2011; Tamsitt et al., 2017). The ACC south of Tasmania (around 55°S, 150°E) is a region of strong eddy kinetic energy (EKE) due to the interaction of the current with the Southeast Indian Ridge. Downstream of the ridge, the fronts form standing meanders that generate mesoscale eddies and intense meridional fluxes of heat and other tracers (Patel et al., 2019, 2020; Rees et al., 2019; Ries et al., 2009; Wolfe & Byrne, 2016). This mesoscale variability has been suggested to impart more variability on the macronutrient and iron supply (Garabato et al., 2001; Lannuzel et al., 2011; McGillicuddy, 2016; McGillicuddy et al., 1998).

Phytoplankton blooms are closely related to mesoscale activity (Abbott et al., 2000; Grenier et al., 2015; Kahru et al., 2007). Eddies can redistribute biomass through eddy trapping and stirring, and enhance phytoplankton productivity through eddy pumping (Gaube et al., 2014; Kahru et al., 2007; McGillicuddy, 2016). Cyclonic eddies can enhance the macronutrient and iron concentration and maintain phytoplankton in the surface layer by lifting isopycnals, during formation while anticyclonic eddies do the opposite (Abbott et al., 2001; Moreau et al., 2017). Many studies have shown that cyclonic eddies enhance phytoplankton growth (Jones et al., 2015; Kahru et al., 2007; Patel et al., 2020), while others suggested that anticyclones and frontal structures may do the same (Abbott et al., 2000; Barré et al., 2011; Song et al., 2016). Upwelling generated by eddies can provide an important iron input, locally enhancing phytoplankton physiology (Behrenfeld et al., 2006; Bowie et al., 2009; Boyd & Abraham, 2001; Ellwood et al., 2008; Viljoen et al., 2018). In addition to their impact on phytoplankton productivity, eddies can impact the biological carbon pump via physical processes. It is believed that both cyclones and anticyclones can switch between being carbon sources and carbon sinks depending on the season (Jones et al., 2015; Moreau et al., 2017; Song et al., 2016), because the dissolution of dissolved inorganic carbon (DIC) depends on temperature and alkalinity. The upwelling or advection generated by eddies may change the local carbon pump by varying the contrast with DIC-rich water. Therefore, air-sea CO_2 exchange depends on the coupling between the biological pump and the solubility pump, and the way in which both are impacted by eddies.

The Southern Ocean is very sensitive to wind and buoyancy forcing. While the ACC has been experiencing stronger westerly winds over the last few decades, most of this additional energy has been seen in increased EKE, instead of ACC transport (Böning et al., 2008; Hallberg & Gnanadesikan, 2006; Marshall et al., 2017; Munday et al., 2013). Specifically, eddy hotspots like the PF standing meander may become more active and subject to change in the future (Bischoff & Thompson, 2014; Meredith & Hogg, 2006; Thompson & Garabato, 2014; Williams et al., 2007). The increase in EKE is likely to affect both the rate of property transport across the ACC and the upwelling of CDW. Considering that mesoscale structures are closely related to blooms, standing meanders may be a window for us to observe the response of biogeochemical properties to variability in the Southern Ocean, and the key to understanding future changes in the carbon budget. Therefore, this study is aimed at:

1. Understanding how the physical environment drives phytoplankton biomass distribution, and to what extent biological activity can affect local carbon sink characteristics.
2. Characterizing phytoplankton physiology and its response to mesoscale physics in the HNLC PF meander.
3. Investigating the generally low productivity in the area and determining drivers of interannual variability.

2. Data and Methods

2.1. Data Sources

2.1.1. Voyage Data

From 16 October to 15 November 2018, voyage IN2018_V05 on RV Investigator surveyed a standing meander of the PF south of Tasmania, approximately 146°–158°E, 52.5°–57.5°S (Figure 1). The goal of this voyage was to obtain observations of the spatial structure and temporal variability of the PF standing meander, to examine the physical processes that contribute to poleward fluxes of heat and tracers and the downward flux of momentum. Comprehensive biogeochemical measurements were made to investigate the effect of these physical processes on biogeochemistry in the meander.

Surface underway measurements of salinity, temperature, and the partial pressure of CO_2 (pCO_2) were collected during the entire voyage, by standard instrumentation from the underway seawater stream, as described in Moreau

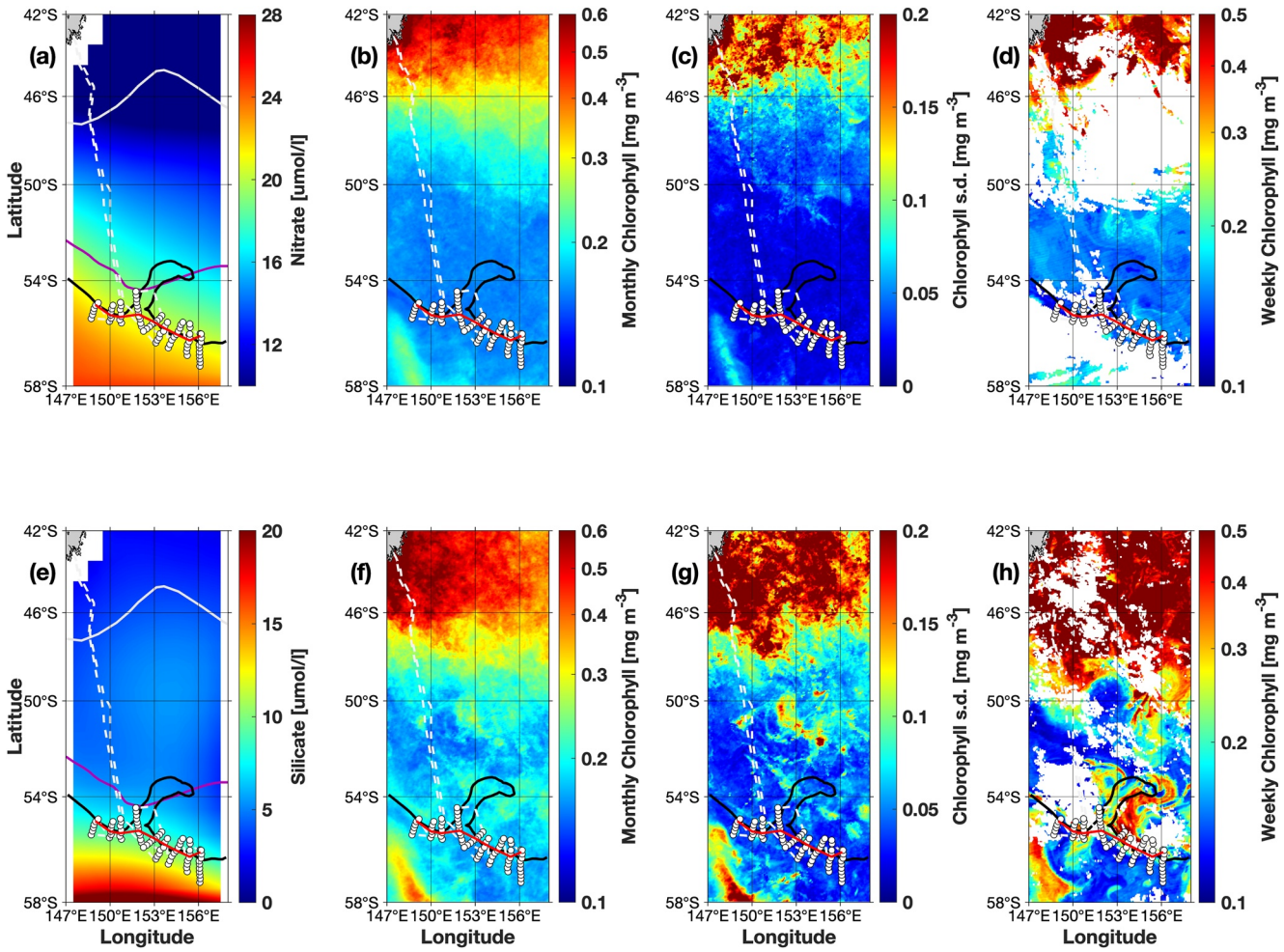

Figure 1. Climatological surface (a) nitrate and (e) silicate concentration for October and November, averaged. The white and magenta lines indicate the climatological position of the Subtropical Front and Subantarctic Front, respectively (Orsi et al., 1995). Mean (b, f) and standard deviation (c, g) of monthly chlorophyll for October and November, respectively, for the period 2002–2019. Weekly satellite surface chlorophyll for the first (d) and fourth (h) week of the voyage period (October-November 2018). Black line indicates the core of Polar Front (PF) in 2018 defined by a sea surface height value of −0.5 m and the red line indicates the PF core based on the temperature minimum method. White dashed line and white circles indicate the voyage track and conductivity temperature depth (CTD) stations, respectively.

et al. (2017). The phytoplankton photochemical efficiency was defined by normalized variable fluorescence (Fv/Fm; Behrenfeld et al., 2006). Fv/Fm was measured by a Satlantic Fluorescence Induction and Relaxation (FIRe) system in the shipboard underway laboratory. The flash sequence was set to single turnover flash/single turnover repetition (STF/STRP) with 40 saturation flashes, 40 ms relaxation duration, 50 µs initial flash interval and 30 iterations (number of measurements averaged for each reported data point).

There were 77 conductivity temperature depth (CTD) casts to within 10 m of the sea floor (~4,000 m), including hydrochemistry. The CTD casts were conducted along nine cross-front transects using a Seabird SBE911 CTD unit, with 36 12 L bottles on the rosette sampler. Water samples (500 mL) were filtered, and the chlorophyll extracted in 90% acetone at −20°C for at least 24 hr before being analyzed in a Turner Trilogy fluorometer that was calibrated with known standards (Strutton et al., 2004). Nutrient samples were analyzed on board using an ALP-kem rapid flow analyzer (Rees et al., 2019). Pressure (depth), temperature, conductivity (salinity), and dissolved oxygen were computed based on the calibration factors supplied by Seabird and the CSIRO. Potential density was calculated from temperature and salinity using the Gibbs Sea Water package in Matlab and was used to calculate the mixed layer depth (MLD), for the nutrient drawdown calculations (Section 2.2.4; McDougall & Barker, 2011). The uncertainty of the nutrient measurements was as described in Hughes et al. (2018).

2.1.2. Ancillary Satellite, Climatological, and Argo Data

Weekly surface temperature data and surface chlorophyll concentration for the voyage period were collected by the NASA Visible and Infrared Imager/Radiometer Suite (VIIRS) mission. The monthly chlorophyll climatology from 2002 to 2019 and the monthly average chlorophyll concentration were collected by the NASA Moderate Resolution Imaging Spectroradiometer (MODIS) mission. The chlorophyll data have a spatial resolution of 4 km. We acknowledge that the voyage period and the climatology/historical data were from different sensors, but this was done to provide the best quality contemporary data and also the longest historical record. The DUACS provided daily sea surface height (SSH) data, geostrophic current velocity and wind speed at 0.25° spatial resolution.

Climatological nutrient data were obtained from NOAA's World Ocean Atlas 2018 (WOA18) at 1° spatial resolution. These data were used to understand the background nutrient conditions of the region. The Roemmich-Gilson Argo Climatology product provided full-depth temperature and salinity data from 2004 to 2019, with a spatial resolution of 1° (Roemmich & Gilson, 2009). The eddy climatology data were obtained from AVISO+.

2.2. Data Analysis

2.2.1. Biogeochemical Climatologies

The average climatological nitrate and silicate for October and November from WOA18 were further averaged across both months to create a distribution indicative of the period of the voyage in the PF area (Figures 1a and 1e). To understand the climatology and variability of chlorophyll in the PF meander, the monthly climatology of October and November chlorophyll from 2002 to 2019, and its standard deviation were mapped (Figure 1b, 1c, 1f, and 1g).

2.2.2. Definition of PF Location, CDW, and Euphotic Zone Depth

We defined the location of the PF using two methods. The first defines the PF as the northernmost position of the 2°C isotherm in the temperature minimum layer (Talley et al., 2011). The vertical temperature profiles collected by CTD stations along nine transects were interpolated to determine the accurate position of the PF core based on this definition (red line in Figure 1). Second, consistent with previous work on this survey data (Wang, 2020) we chose an SSH contour of −0.5 m to mark the PF core (black contour in Figure 1). Except for transects 4 and 5, the position of the PF core defined by these two methods corresponds well.

The CDW is indicated as the upwelled water with oxygen concentration below 200 μmol kg^{-1} (Wang, 2020). The euphotic zone depth was calculated based on the total chlorophyll with functions:

1. $Ze = 912.5*[Chl_{tot}]\text{^}-0.839$ $\quad 10\ m < Ze < 102\ m$
2. $Ze = 426.3*[Chl_{tot}]\text{^}-0.547$ $\quad 102\ m < Ze < 180\ m$

where Ze is euphotic zone depth (m) and Chl_{tot} is integrated chlorophyll (mg m^{-3}; Morel & Maritorena, 2001; Su et al., 2021).

2.2.3. Phytoplankton Physiology

Surface underway Fv/Fm was measured about every 5 s, and we calculated a 60-min moving average every 10 min after removing bad data. Sunrise and sunset times were calculated using the Matlab sunrise toolbox and were used to distinguish day and night Fv/Fm data. To avoid the influence of nonphotochemical quenching, only night time Fv/Fm data were plotted in underway maps. Behrenfeld et al. (2006) suggested that the dawn maximum and the nocturnal decrease in Fv/Fm are important indices for physiological characteristics. The maximum in the 2-hr window before and after sunrise was used to define the dawn maximum. The nocturnal decrease was defined by the ratio of the nighttime minimum value to the average value of Fv/Fm at the neighboring sunrise and sunset. Following Behrenfeld et al. (2006), we chose 25% as the threshold for determining a large nocturnal decrease. But because the Southern Ocean has a much higher surface macronutrient concentration than the equatorial Pacific, we chose Fv/Fm = 0.5 as the threshold to indicate a high dawn maximum, instead of 0.45 used by Behrenfeld et al. (2006).

2.2.4. Nutrient Deficits and Organic Carbon Production

The seasonal drawdown of nutrients was used to calculate particulate organic carbon (POC) production. For a given CTD location, the nutrient deficit was defined as the difference between the nutrients in the temperature minimum (T_{min}) layer and the mixed layer (Jennings et al., 1984). We defined the MLD in this area as the depth where the potential density increased by 0.02 kg m^{-3} with reference to a near-surface (10 m) density. In cases where CTD data were missing at 10 m, we selected the shallowest value (varied from 11 to 31 m). Because of deep winter mixing, the nutrients in remnant Antarctic Winter Water (AWW, the T_{min} layer) are indicative of the surface nutrient concentration before the start of the growing season. The average of all nutrient samples in the mixed layer was considered as the nutrient concentration after consumption. To help reduce biases due to nonuniform sampling in the vertical, the CTD bottle nutrient samples above 600 m were linearly interpolated to 1-m resolution. POC production was calculated by multiplying the seasonal nitrate drawdown by the Redfield C:N ratio (106/16). This method may not perform well at the intersection of different water masses, such as at the core of the PF, so the seasonal drawdown of macronutrients has only been determined for the southern part of the CTD transects.

3. Results

3.1. Climatological Nutrient and Chlorophyll Distributions Around the PF Meander

Strong south-north decreasing gradients were observed in surface macronutrient climatological distributions (Figures 1a and 1e). A front in macronutrients also existed near the PF meander, where nitrate varied from about 22 to 19 μmol L^{-1} and silicate from about 13 to 7.5 μmol L^{-1}. Large-scale gradients were also observed in the chlorophyll climatology, but the highest concentrations appeared at the subtropical zone (STZ) in the lowest macronutrient waters (Figures 1b and 1f). To investigate the relationship between macronutrient variation and chlorophyll distribution, historical satellite chlorophyll data were mapped (Figure 1 and Figure S1 in Supporting Information S1).

In October, based on the climatology, the average chlorophyll along the whole PF meander region is quite low (about 0.15 mg m^{-3}) and its standard deviation approaches zero, which indicates that there is no frequent bloom in this area. However, southwest of the PF meander, around 148°E, 57°S, chlorophyll is slightly higher, about 0.25 mg m^{-3} and the standard deviation is also higher. This suggests a regular bloom that starts to occur in October (Figures 1b and 1c and Figure S1 in Supporting Information S1).

In November, higher average chlorophyll and stronger variability (higher standard deviation) were observed in the whole area, especially in the southwest corner (mean chlorophyll about 0.4 mg m^{-3}) and STZ (mean chlorophyll over 0.5 mg m^{-3}; Figures 1f and 1g). In both areas, the standard deviation was over 0.2 mg m^{-3}. All these data suggest regular strong bloom events. In contrast, we did not observe high average chlorophyll along the PF meander, and a spring bloom was only observed in a small number of years (Figure S1 in Supporting Information S1). In 2018, the surface chlorophyll concentration was over 0.5 mg m^{-3} which we considered to be an abnormal event. It was likely caused by factors other than the meridional gradient in macronutrients.

3.2. Chlorophyll, Temperature, and SSH Distribution During the Voyage: The Influence of Eddies and Frontal Process

We used SSH, sea surface temperature (SST), and geostrophic currents (Dong et al., 2011; Du et al., 2019; Zhang et al., 2014) to understand physical drivers of the distribution of surface chlorophyll, and to define eddies (Figures 2 and 3). A cyclonic eddy arose northeast of the PF trough (the northward excursion of the meander) near 154°E, 54°S in the third week of the voyage, with SST about 3°C and SSH about −0.8 m at its center (Figures 2a and 2b). The SSH and geostrophic velocity fields suggest the eddy had not yet completely separated from the front at that time. East of the forming cyclonic eddy, there was a strip of warm water at the outer edge of the cyclonic flow and northward flow further east, suggesting an anticyclonic meander bringing warmer water southward. In week 4, an anticyclonic eddy appeared in the location of the southward limit of the warm water, north of transects 8 and 9 (Figure 2d, near 156°E). Although the measurements were affected by clouds, this eddy captured warm surface water, about 8°C, and had an SSH of about +0.20 m (Figures 2c and 2d). The cyclone mentioned before moved eastward to around 156°E, 54°S, with SST about 3°C and SSH about −0.7 m

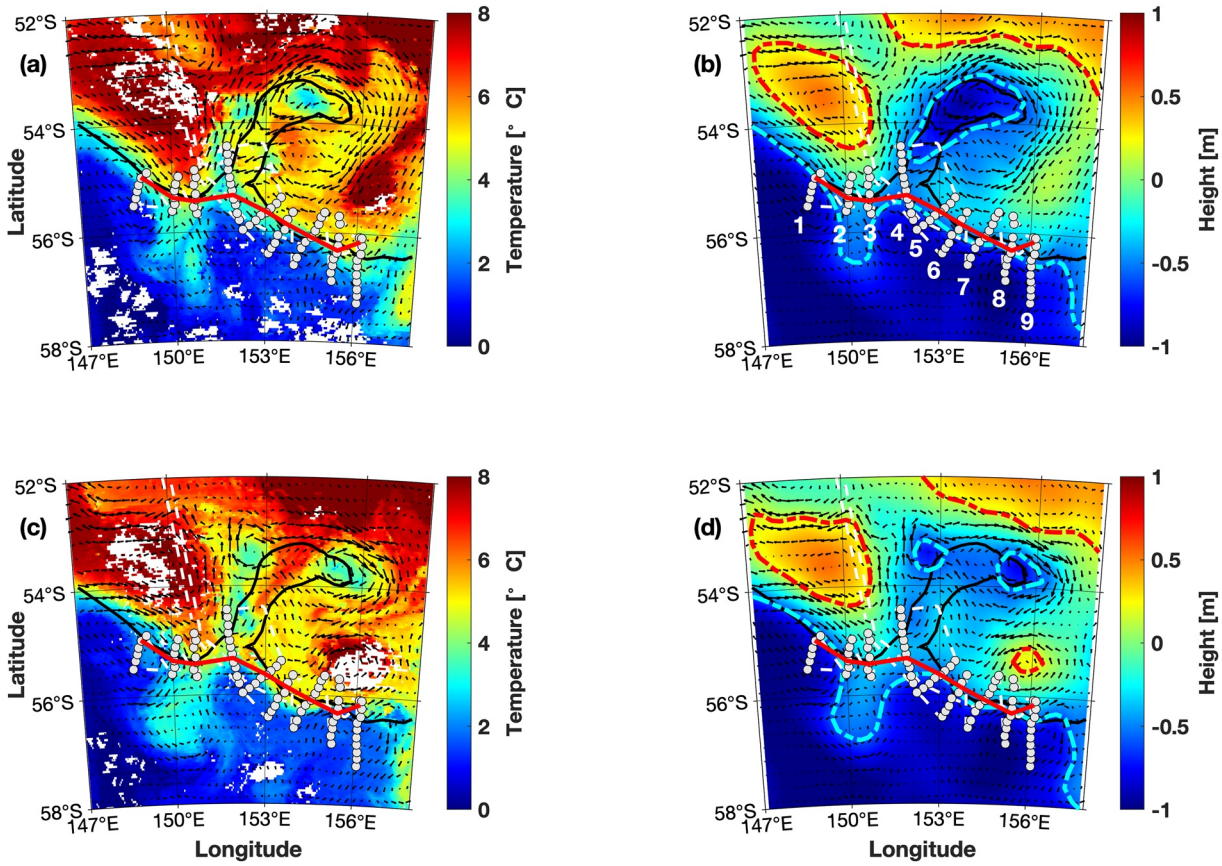

Figure 2. (a and c) Sea surface temperature (SST) and (b and d) sea surface height (SSH) maps of the study area during week 3 (1 November 2018 to 8 November 2018, upper panels) and week 4 (9 November 2018 to 16 November 2018, lower panels) of the voyage. The weekly average geostrophic current is indicated by black arrows. The ordering of conductivity temperature depth (CTD) transects are marked in (b). The cyan and red dashed contours indicate SSH of −0.6 and 0.17 m, respectively, to illustrate the general position of anticyclonic and cyclonic eddies (b) and (d). The Polar Front (PF), CTDs, and voyage track are as described in the previous figures.

(Figures 2c and 2d). A new cyclone formed to the west of the PF trough (around 152.5°E, 53.5°S), with SST and SSH characteristics similar to the other cyclone (Figure 2d).

The week-by-week development of the bloom during the voyage is shown in Figure 3. In the first 2 weeks, no bloom was observed in the upstream (western) area (transects 1 through 4; Figures 3a and 3b). In the last 2 weeks of the voyage, when the ship was in the downstream region (east of about 151°E), satellite images show that high chlorophyll began to appear along the SSH contour marking the front (Figures 3c and 3d). In Figure 3d, there are several areas of high chlorophyll. The first is located east of 153°E and rotates with a low-chlorophyll core at 156°E, 54°S with quite high chlorophyll (>0.5 mg m^{-3}) to its south. The other is a narrow strip west of 153°E with lower chlorophyll (about 0.3 mg m^{-3}), and spinning around a core at about 152°E, 53°S. In addition to the bloom surrounding the eddies, we also observed a narrow strip with chlorophyll over 0.4 mg m^{-3} along the PF track, which developed since the second week (Figures 3b–3d). These high chlorophyll areas corresponded well to the edge of cyclonic eddies and the PF (Figures 2 and 3). At 156°E, 55°S, there was an area of low chlorophyll (close to 0.1 mg m^{-3}), in the anticyclone east of the meander (Figures 3d and 9f).

3.3. Phytoplankton Physiology From Underway Measurements

During the whole voyage, the Fv/Fm nocturnal decrease was generally small, except for one anomaly measured at about 149°E, 55°S (Figure 4b). Spatial variability in the dawn maximum was more pronounced. Based on the Fv/Fm features, there were two physiological regions that could be distinguished during the voyage (Figure 4). The first of these included the outbound transect (from Tasmania to the survey area), the return transect, and

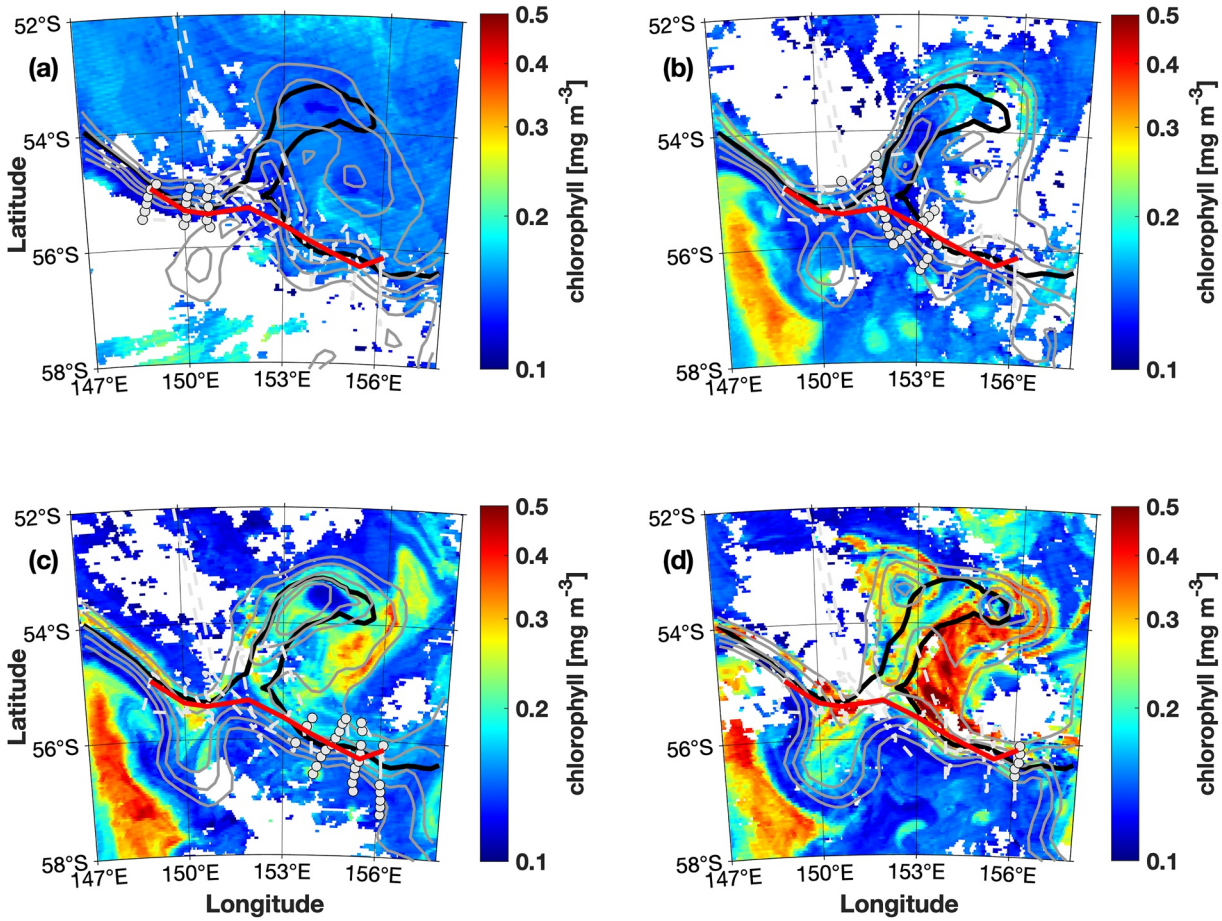

Figure 3. Weekly satellite surface chlorophyll maps of the area for the 4 weeks of the voyage. (a) week 1, 16 October 2018 to 23 October 2018; (b) week 2, 24 October 2018 to 31 October 2018; (c) week 3, 1 November 2018 to 8 November 2018; (d) week 4, 9 November 2018 to 16 November 2018. The Polar Front (PF), conductivity temperature depths (CTDs), and voyage track are as described in the previous figures, except that only the CTDs that were performed in the relevant time window are plotted as white circles. The gray contours are the weekly average sea surface height (SSH) from −0.8 to −0.2 m with 0.1-m interval.

the northern part of the downstream survey area, which were characterized by small nocturnal decrease (<25%) and relatively high dawn maximum (>0.5). The upstream and southern part of the downstream survey area were characterized by small nocturnal decrease and relatively low dawn maximum (<0.5). Compared with Section 3.2,

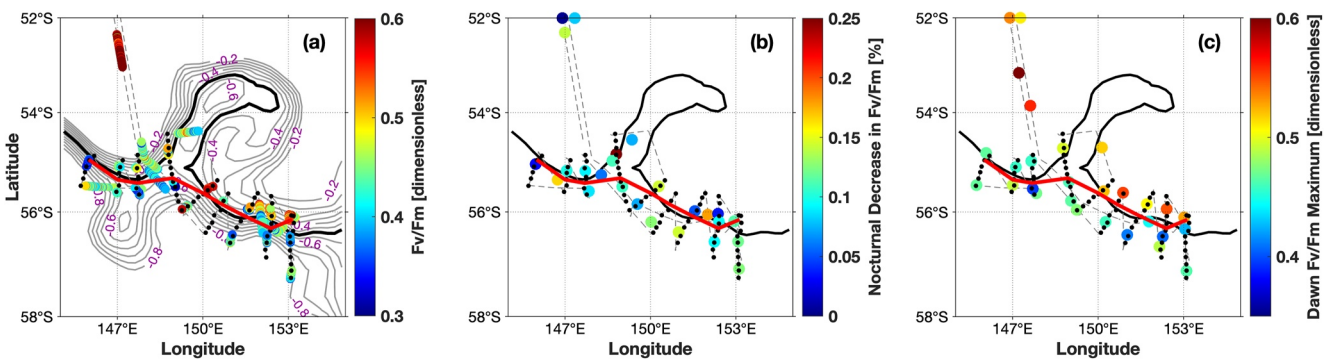

Figure 4. Phytoplankton physiological characteristics along the voyage track. (a) Underway night time Fv/Fm 60 min moving average value, (b) nocturnal decrease, and (c) dawn maximum. The contours in (a) are mean SSH for the voyage period, to show the range of the PF meander. The core of the PF defined by the −0.5 m SSH is the thick black contour. The PF defined by the T_{min} method is the red line. The CTD stations are indicated by the black dots.

these results demonstrate more biomass with a healthier phytoplankton community in the downstream northern area and the transit to and from the study area.

Although the ship tracks to and from the study area mainly passed through the same region, there were still differences between them regarding phytoplankton physiology. The Fv/Fm values were more variable on the return transect, and they were generally lower than the outbound transect until 16 November 2018 (Figure S2 in Supporting Information S1). A similar phenomenon also appeared in dawn maximum and nighttime Fv/Fm (Figures 4b and 4c). The satellite measurements showed that on the return transect approaching Tasmania, the bloom in the STZ was strengthening. The Fv/Fm increased north of 47°S on the return transect, exceeding the values of the outbound transect at 44°S to reach about 0.64 near Tasmania. The dawn maximum also increased in the same area (Figure S2 in Supporting Information S1; Bindoff & Phillips, 2019).

3.4. Result From CTD Transects

3.4.1. Macronutrient Distributions

Nine sections of hydrography collected by CTD stations illustrate the distribution of dissolved nitrate, ammonium, silicate, and chlorophyll. We numbered the transects from 1 to 9 (Figure 2b), and chose transects 3 and 9 as representatives of the upstream and downstream region, respectively (Figures 5 and 6, Figures S3–S9 in Supporting Information S1).

In general, nitrate was very high below about 200 m south of the PF. The peak value was over 36 μmol L^{-1} at the depth limit of the sections depicted here (300 m). The lowest concentrations, about 25 μmol L^{-1}, usually occurred at the surface, north of the PF. The interior distribution of nitrate was closely aligned to the structure of isopycnals, especially below the mixed layer (100 m). For example, the 32 μmol L^{-1} nitrate isopleth almost coincides with the 27.2 kg m^{-3} isopycnal (Figure 5). The distribution of silicate was similar, but its concentration ranged from 5 to 60 μmol L^{-1}. The north-south decreasing gradient of nitrate and silicate was consistent with the surface climatology (Figures 1a and 1e).

The ammonium distribution varied considerably between transects. The concentration of ammonium in transects 1 to 3 was not more than 0.2 μmol L^{-1} (Figure 5, Figures S3 and S4 in Supporting Information S1). Relatively high concentrations were found at about 100 ± 50 m and lower concentrations at the surface and below 200 m. As the ship moved downstream in the ACC, the concentration increased. Water masses with high ammonium were found near the PF and the southern end of the transects (Figure 6, Figures S7–S9 in Supporting Information S1). For example, in transect 9, a high ammonium (>3.5 μmol L^{-1}) layer was found aligned with the 27.5 kg m^{-3} isopycnal, which dipped below 200 m at the PF, and was unique in all transects (Figure 6).

3.4.2. Biomass Distribution

For all transects, chlorophyll was confined to the surface mixed layer, above ~100 m (Figure 7). We observed three kinds of patterns. In the first two transects, the chlorophyll concentration was generally low. The surface chlorophyll varied between 0.3 and 0.4 mg m^{-3}, except at the southern end of transect 1 (Figures 7a and 7b). For transects 3–6, some water masses had a relatively high chlorophyll concentration, about 0.5 mg m^{-3} (Figures 7c–7f). These mainly appeared in the PF and near the ends of some transects. A bloom was observed in the last three transects, especially near the PF, and chlorophyll concentration was greater than 0.65 mg m^{-3} (Figures 7g–7i). The distribution of this high chlorophyll was very narrow, and there was a strong gradient toward the surrounding water masses.

3.5. Carbon Properties

Like macronutrients and chlorophyll, surface pCO_2 exhibited a strong south to north gradient from about 410 ppm in the PF area to about 330 ppm in the STZ (Figures 1 and 8a). Around 46°S, when the ship returned to Tasmania, lower pCO_2 was observed compared to the southbound transect, which was largely driven by the rapid increase in productivity during the voyage period (Figures 1d and 1h). In the study region, the surface pCO_2 was higher in

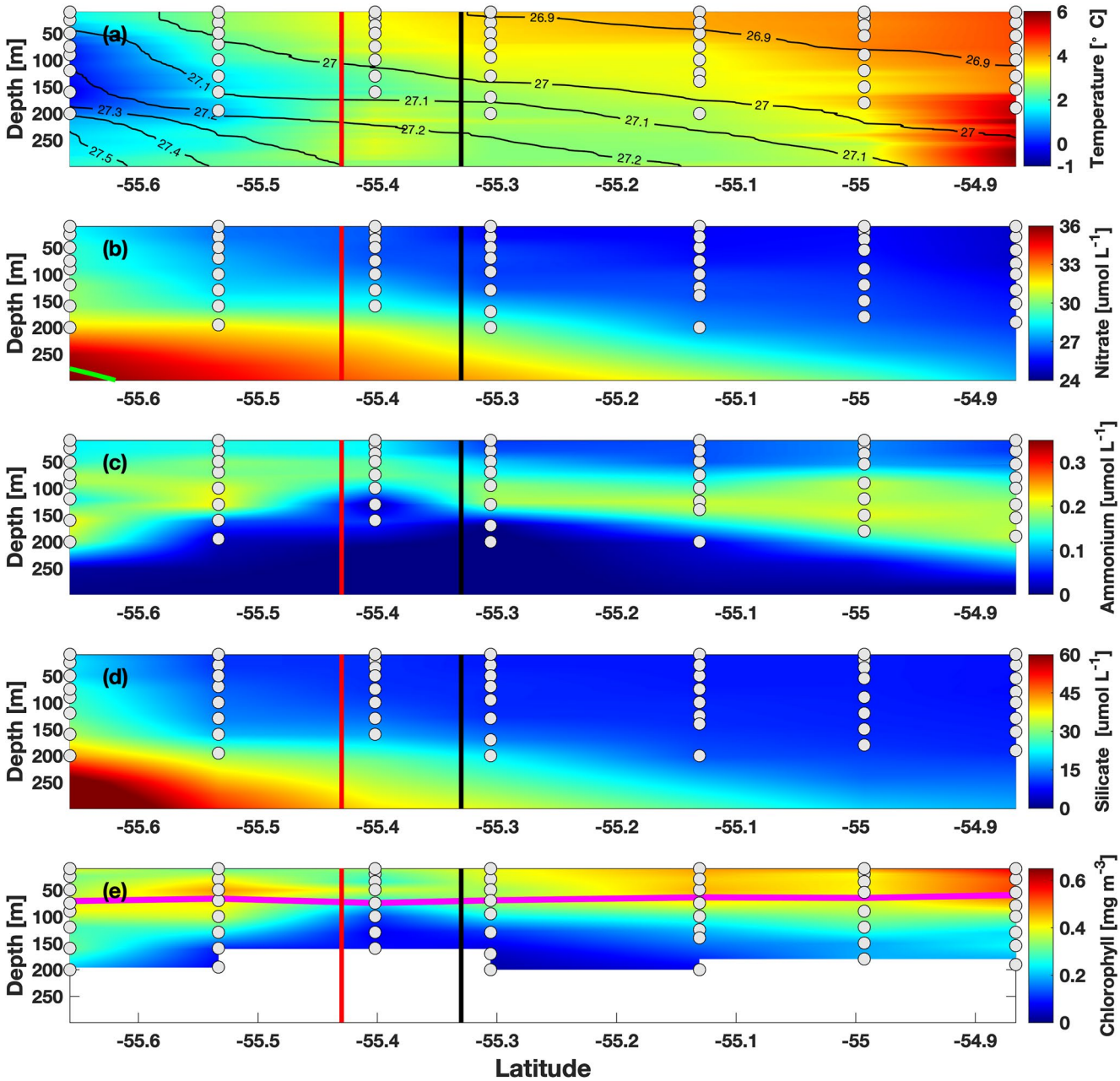

Figure 5. Depth-latitude plots from conductivity temperature depth (CTD) transect 3, (a) temperature (°C) with potential density (kg m^{-3}) as black contours; (b) nitrate (μmol L^{-1}), the green contour indicates the upper boundary of Circumpolar Deep Water (CDW); (c) ammonium (μmol L^{-1}); (d) silicate (μmol L^{-1}); and (e) chlorophyll (mg m^{-3}), the magenta line indicates Ze. CTD bottle samples are indicated by white circles. The red vertical line indicates the Polar Front (PF) core defined by the minimum temperature method and the black vertical line is the PF core defined by SSH = −0.5 m.

the downstream area compared to that of the upstream, especially for transects 5–8 (Figure 8b). The water mass with highest pCO_2 was observed around 154°E, 56°S (between transects 6 and 7), with a concentration of over 425 ppm. At the easternmost end of the study area, pCO_2 slightly decreased to about 400 ppm in the northern part of transect 9. When the ship returned to the anomalously high pCO_2 region, pCO_2 had decreased about 30 ppm.

Strong gradients were found in the biological carbon production map (Figure 8c). The productivity was generally low in the first five transects, with values varying between 0 and 20 μmol L^{-1}. In contrast, productivity increased in the last four transects, to about 40 μmol L^{-1} at some sites. The carbon production gradually increased eastward,

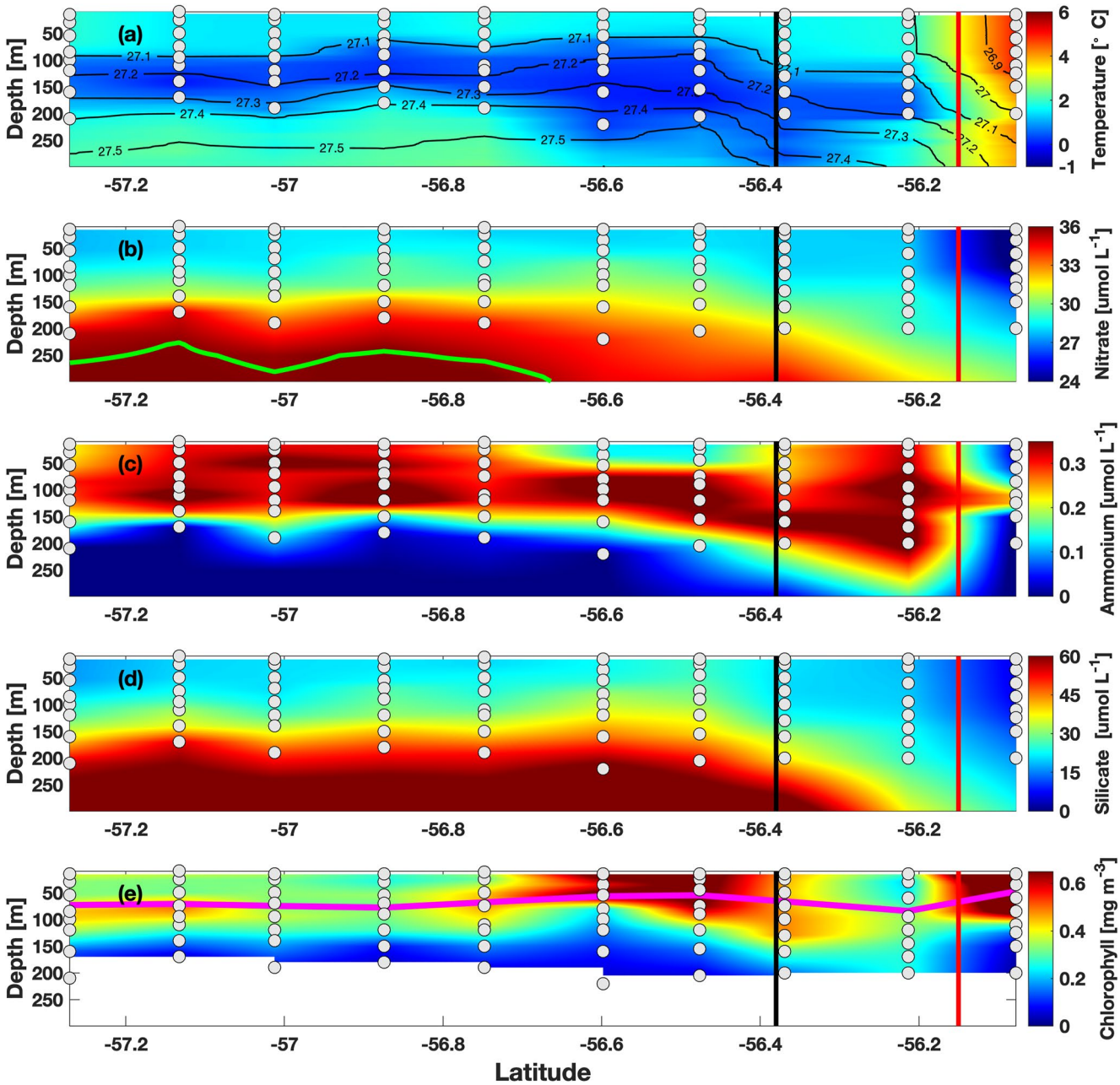

Figure 6. Same as Figure 5, but for conductivity temperature depth (CTD) Section 9.

contrary to the trend of surface pCO_2, as expected, indicative of strong drawdown. Interestingly, extremely low carbon production was observed at the PF on each transect.

3.6. Correlation Between MLD, Eddies, and Biomass From Argo and Satellite Observations

The intensity of the bloom in our study area has varied over our retrospective 2002 to 2019 analysis, and 2018 appears to have been an exceptional year (Figure S1 in Supporting Information S1). In the following, we use MLD calculated from the RG-Argo monthly data. We investigated whether the MLD difference between October and November ($MLD_{diff} = MLD_{Oct} - MLD_{Nov}$), and the number, location, and polarity of eddies are possible drivers of the interannual variability and present summary statistics in Table S1 in Supporting Information S1. Generally,

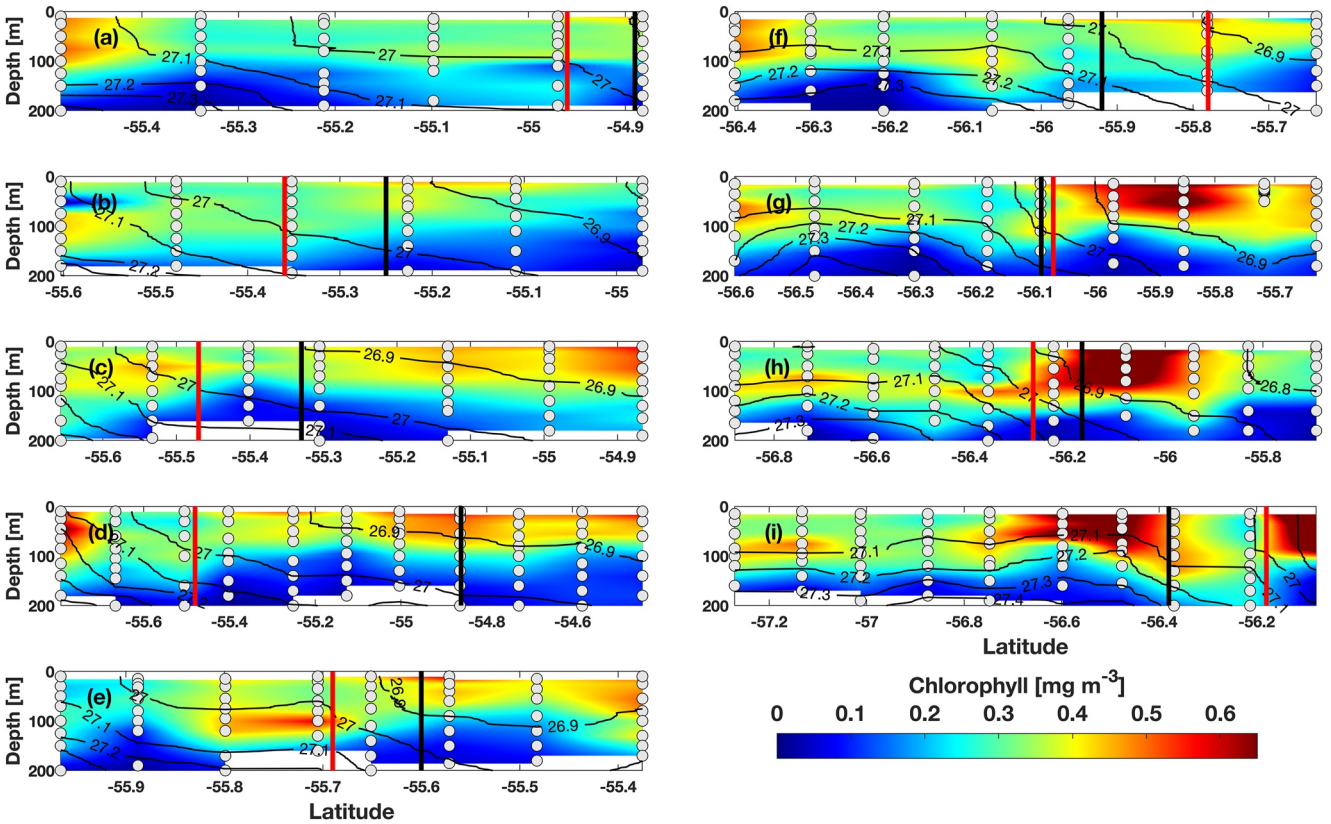

Figure 7. Depth-latitude transects of chlorophyll distribution. Panel (a) to (i) correspond to transects 1–9. The isopycnals, conductivity temperature depth (CTD) stations, and the Polar Front (PF) are marked as in the previous figures.

when the MLD shoaled from October to November (positive MLD_{diff}) induced by seasonal surface warming and increased stratification, the chlorophyll concentration in November tended to increase. In addition, when the study area had strong cyclonic eddy activity and weak anticyclonic eddy activity, phytoplankton biomass tended to be higher (Table S1 in Supporting Information S1). At other times, the chlorophyll was relatively low. To test this, and because we are interested in the bloom to the north and northeast of the PF meander, we defined a polygon within which to quantify chlorophyll, MLD and eddies, by four vertices: 148°E, 53°S; 148°E, 54.5°S; 158°E, 56.5°S; 158°E, 53°S (Figure 9a). A group of case studies showed that when the MLD shoaled in 2017 and 2018 by 112 and 82 m, respectively, and active cyclones were observed, biomass increased (Figure 9, Figures S1, S11, and Table S1 in Supporting Information S1). On the contrary, in 2007, weak MLD shoaling (21 m) and strong anticyclonic activities were observed, which resulted in low chlorophyll (Figure 9, Figures S1, S11 and Table S1 in Supporting Information S1). Across all years, the correlation between MLD_{diff} and chlorophyll was 0.259 ($p = 0.333$; Figures S1 and S11 in Supporting Information S1), indicating that MLD_{diff} has a positive but not statistically significant impact on chlorophyll in November.

4. Discussion

Using ship-based observations, satellite measurements, and nutrient climatologies, we studied a standing meander of the PF south of Tasmania in austral spring 2018 (16 October to 15 November). During this period, we discovered a phytoplankton bloom that was unusually strong in the context of historical observations. Based on SSH and SST anomalies, the voyage sampling took place while at least two cyclonic eddies were forming in the trough (northward extension) of the meander. Therefore, this data set presents a unique opportunity to study biogeochemical variability in the presence of multiple mesoscale structures (eddies and fronts), and their impact on local carbon cycling.

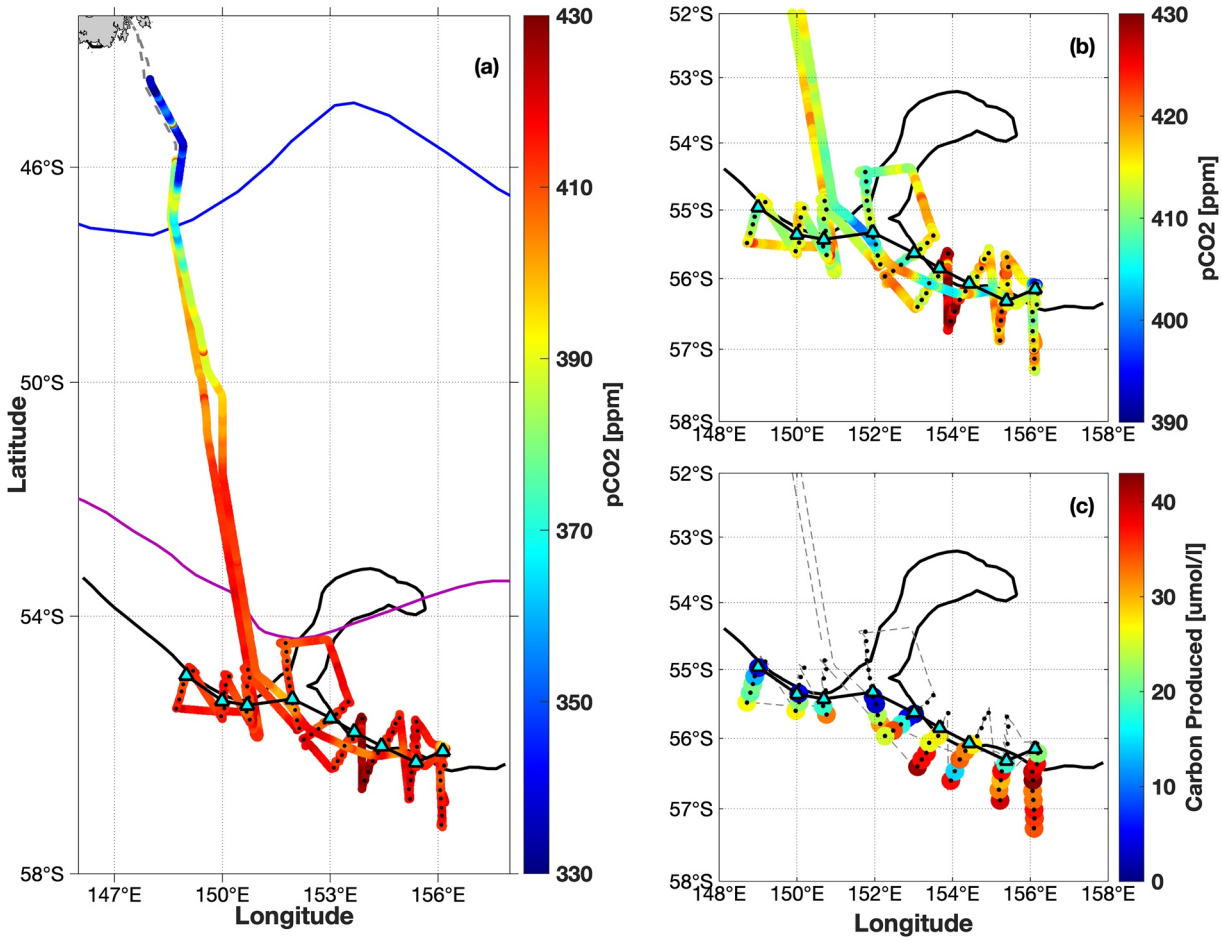

Figure 8. Underway pCO_2 mapping for (a) the whole voyage track and (b) the Polar Front (PF) meander. Carbon production (POC) is mapped in (c). The blue and magenta lines in (a) indicate the climatological position of the Subtropical Front and Subantarctic Front, respectively (Orsi et al., 1995). The PF (black solid lines, with cyan triangles for the T_{min} method) and voyage track (black dotted line) are as described in the previous figures. Conductivity temperature depth (CTD) stations are indicated by black dots.

4.1. Macronutrient and Phytoplankton Biomass Distribution

4.1.1. Macronutrient Distribution

All CTD transects exhibited strong meridional gradients of macronutrients, which was consistent with the climatologies of nitrate and silicate. In this study, we focused on the distribution of macronutrients in the upper 300 m where productivity potentially occurs. There was enrichment of macronutrients south of the PF due to the upward slope of isopycnals to the south and the associated upwelling of nutrient rich CDW, which is also likely to have higher dissolved iron (dFe; Figures 5 and 6, Figures S3–S9 in Supporting Information S1; Ellwood et al., 2008; Schlitzer, 2002; Tang et al., 2021). The concentrations of nitrate and silicate were not biologically limiting (Figures 1a and 1e; Fisher et al., 1992). A regular bloom was mapped with satellite chlorophyll in the STZ, north of about 47°S (Figure 1), confirming that the PF meander was mostly what we consider an HNLC region, and that blooms can occur in the STZ with lower macronutrients, because iron limitation is relieved by the dust source to the north (Bowie et al., 2009; Lannuzel et al., 2011).

The distribution of biomass did not correlate with the subsurface structure of nitrate, silicate or nitrite (nitrite not shown), but it was reflected in the subsurface structure of ammonium (Figures 5 and 6). High levels of ammonium were found under and adjacent to high chlorophyll (Figure 6 and Figures S6–S9 in Supporting Information S1), due to remineralization (Sarmiento & Gruber, 2006). This phenomenon was more noticeable in the downstream transects, because of stronger biological activity (chlorophyll concentration over 0.5 mg m^{-3}; Figures 3 and 7).

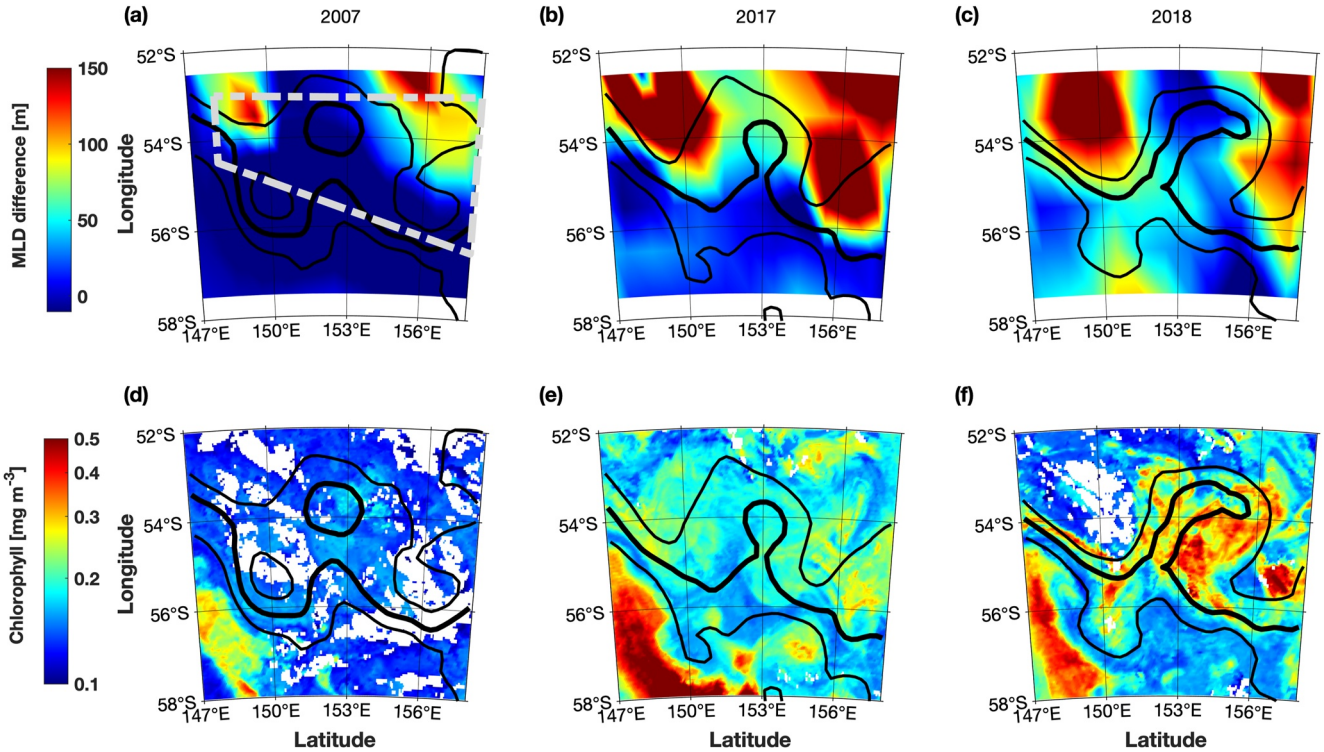

Figure 9. Relationship between MLD_{diff} and chlorophyll in November. The upper panels plot the MLD_{diff} in (a) 2007, (b) 2017, and (c) 2018. The corresponding November chlorophyll is mapped in the lower panels (d, e, and f). The thin contours represent the meander region (SSH = −0.7 to −0.3 m) and the thick contour indicates the Polar Front (PF) core (SSH = −0.5 m). The area used to calculate average chlorophyll and mixed layer depth (MLD) for Table S1 in Supporting Information S1 is indicated with gray dashed polygon in panel (a).

4.1.2. Biomass Distribution and Relationship With Eddies and Frontal Process

Elevated chlorophyll in the PF and eddies suggests that mesoscale structures contributed to the development of this bloom (Figures 2 and 3). Eddies in this region are primarily generated by instability of the ACC fronts. Standing meanders in the fronts are formed where the fronts interact with steep topography and, within the meanders, instability of the front and the generation of eddies is enhanced (Chapman et al., 2015; Frenger et al., 2015; Rintoul, 2018). The eddies that we focused on in this study were formed from the ACC standing meander between the Southeast Indian Ridge and the Macquarie Ridge. Frenger et al. (2015) identified this area as a hotspot for long-lived eddies. This area is far away from terrestrial iron sources and the influence of sea ice (Bowie et al., 2009; Cavalieri et al., 1996; Lannuzel et al., 2011), suggesting that these eddies are produced without iron input from any islands (Moreau et al., 2017). This is in contrast to the situation where high chlorophyll eddies observed near islands like the Kerguelen Plateau, have productivity that is likely enhanced by terrestrial iron (Della-Penna et al., 2018; Grenier et al., 2015).

Although our in situ data are not sufficient to determine the specific generation mechanism, here, we explore the clues that we can identify from the data regarding the development of the strong phytoplankton bloom. Figure S12 in Supporting Information S1 presents schematics to illustrate three mechanisms associated with eddy formation based on McGillicuddy (2016) and the Southern Ocean eddy census of Frenger et al. (2015). Eddy stirring is a horizontal advection of a passive tracer such as chlorophyll, by the rotating eddy, causing patches of high chlorophyll to be carried into regions of low chlorophyll and vice versa (Figure S12a in Supporting Information S1). Eddy trapping occurs when a steep meander in a front pinches off, enclosing water from one side of the front and carrying it to the other side (Figure S12b in Supporting Information S1). Eddy pumping relates to upwelling and downwelling in cyclones and anticyclones, respectively, when an eddy is growing or decaying (Figure S12c in Supporting Information S1). Each of these mechanisms may have played a role in the biomass distribution and the development of the strong phytoplankton bloom during the voyage in the presence of developing eddies.

During the voyage, two cyclones were spawned in the trough of a steep meander in the PF near 52°S, 152°–156°E (Figure 2). In week 3, a cyclonic eddy characterized by low SST, low SSH (Figures 2a and 2b), and low chlorophyll (Figure 3c) appeared near 154°E, indicating eddy trapping. The cyclone developed from the meander stage to the separation stage, pinched off as a ring with cool, low chlorophyll water from south of the PF at its center, and was transported eastward away from the front in week 4. This is similar to the formation and life history of a cyclonic eddy studied in Patel et al. (2019), generated at the Subantarctic Front to the north of our study.

The high chlorophyll around the edge of the cyclonic eddy and PF (Figure 3c) could be influenced by eddy pumping (Figure S12 in Supporting Information S1) or by vertical motion induced by mesoscale processes (Rodríguez et al., 2001). The eddies are identified in Figure S10 in Supporting Information S1 by their cyclonic vorticity, calculated as $vg_x - ug_y$, where subscripts indicate differentiation and (ug, vg) is the geostrophic velocity from altimetry. The water mass structure within the trough and eddies finds its origin at the southern side of the PF and is sampled most closely on the southern sides of transects 4 and 5 in week 2 of the voyage (Figure 3b). The southern sides of transects 4 and 5 are characterized by shallower isopycnals (Figures 7d and 7e) and associated relatively shallow nutricline (Figures S5 and S6 in Supporting Information S1), bringing higher macronutrients into the mixed layer. The nutrient enriched waters are also likely higher in dFe and could act as an iron source in this open ocean environment (Bowie et al., 2009; de Baar et al., 1990; Ellwood et al., 2008), to boost biomass rapidly (Eveleth et al., 2017; Viljoen et al., 2018).

Frontal processes and eddy stirring may also contribute to generating an environment that could support the bloom. In week 3, as the chlorophyll bloom was getting started (Figure 3c), relative vorticity of the surface flow was strongly cyclonic (negative, Figure S10a in Supporting Information S1) throughout the trough and to the north where the cyclonic eddies formed, with anticyclonic relative vorticity on the warm side of the PF. Near transects 5–7, around 154°E, 55°S, anticyclonic relative vorticity was particularly strong. In week 4, the relative vorticity maxima became more localized to the positions of the eddies, shown in Figure S10b in Supporting Information S1 as "C" for the northern cyclones and "AC" for the anticyclone further south. Strass (1992) discussed the role of frontogenesis in leading to upwelling on the anticyclonic side of an accelerating front leading to chlorophyll blooms. The anticyclonic side of the PF and the outside of the cyclonic eddies are where the highest chlorophyll concentrations occur (Figures 3c and 3d). Upwelling associated with frontogenesis could be a potential mechanism for delivering nutrient rich deeper waters to the mixed layer to support the strong bloom we observed.

Vertical velocity in the ocean has been observed to be linked to the phase of meanders in the Gulf Stream (Lindstrom et al., 1997) and ACC (Phillips & Rintoul, 2000; Watts et al., 2016). These studies show that rotation of the horizontal current drives anomalies in temperature and salinity and vertical motion along isopycnals such that, for the southern hemisphere, there is downwelling leading out of a meander crest and into the trough and upwelling leading out of the trough and into the next crest. Meijer et al. (2022) linked these subsurface relationships to patterns of divergence in surface velocities from a gradient wind balance applied to SSH. The ageostrophic component of the flow reveals deceleration of the current in the trough and acceleration in the crest of the meander. The result is convergence of the flow leading into a trough and divergence leading out of a trough and into a crest. From their detailed hydrographic survey, Meijer et al. (2022) linked along-front variations in water mass properties to show that upwelling along isopycnals is associated with divergence at the sea surface. Applying this theory to our study, we would expect to see divergence and upwelling leading into the crest near 150°E and leading out of the trough and into the next crest, which is where we see the strongest blooms.

There were also other occurrences of high chlorophyll southwest of the meander (around 151°E, 56°S) and along the PF upstream of the meander, which could be contributed by the upwelling of CDW along the front. Further, the surface chlorophyll maps clearly show the rotational flow of the cyclones advecting filaments of high chlorophyll around the eddies, which might have come from the frontal region (Figure 3; McGillicuddy, 2016). Thus, it is likely that both the frontal processes and eddy stirring played roles in stimulating and maintaining this bloom.

Although wind-induced Ekman pumping can lead to downwelling in cyclones, potentially weakening the bloom, we believe it was not an important factor in this study (Gaube et al., 2013; Mahadevan et al., 2008). Wind-induced downwelling is about 0.1 m d^{-1} (Gaube et al., 2013, 2015; Martin & Richards, 2001), much smaller than that of typical eddy-induced upwelling (1–10 m d^{-1}; Lévy et al., 2012, 2001; Mahadevan et al., 2008; Martin & Richards, 2001). Wind-induced downwelling can be influential at the time scale of an eddy's entire life, but eddy-induced upwelling dominates during eddy formation, which we sampled (Martin & Richards, 2001;

McGillicuddy, 2016). It is also possible that submesoscale upwelling around the edge of the eddy stimulated productivity (Lévy et al., 2001, 2012), but we have no direct evidence of that. The new SWOT (Surface Water Ocean Topography) satellite mission may provide valuable detail on submesoscale structures.

4.2. Physiological Characteristics

In this section, we infer the input of dFe to the surface and the relief of iron limitation based on the changing characteristics of phytoplankton physiology. A conceptualized relationship of phytoplankton cells' reaction to the changes in macronutrients and dFe was provided by Behrenfeld et al. (2006). They defined four regimes (I through IV) as a function of the Fv/Fm dawn maximum, nocturnal decrease, the level of oligotrophy and iron limitation (Figure S13 in Supporting Information S1). We did not have trace metal observations on the voyage. However, based on the Fv/Fm determined in Section 3.3 (Figure 4), we surmise that Regime I (iron sufficient, low macronutrients, small nocturnal decrease, high dawn maximum) and Regime IV (iron limited, high macronutrients, small nocturnal decrease, low dawn maximum) best describe the conditions experienced around the PF meander. During the whole voyage, nocturnal decreases were small, thus the dawn maximum was key to distinguishing between Regimes I and IV. The dawn maximum exhibited strong differences between the PF and the northern area (Figure 4, Figure S2 in Supporting Information S1). Macronutrient limitation has been ruled out (refer to Section 4.1), so we infer that dFe was the key driver of phytoplankton physiology. Generally, dFe decreases from north to south (Lannuzel et al., 2011), because of distance from the terrestrial iron input and the iron-rich subtropical waters (Bowie et al., 2009; Ellwood et al., 2008). The southward decrease in dFe enrichment identified in these earlier studies may help to explain the southward decrease in the dawn Fv/Fm maximum (Figure 4c).

In the upstream region of the study area, the PF was characterized by a small Fv/Fm nocturnal decrease and low dawn maximum (Regime IV). In the area closer to the developing eddy, near 150°E and on the equatorward side of the PF in the downstream region, the dawn maximum increased to above 0.5 and the overall value of Fv/Fm increased (Figure 4 and Figure S2 in Supporting Information S1). This is consistent with iron enrichment experiments in the equatorial Pacific (Behrenfeld et al., 2006), South Atlantic (including the PFZ and AZ; Viljoen et al., 2018) and the Australian sector of the Southern Ocean at 140°E, 61°S (Boyd & Abraham, 2001; Boyd & Law, 2001). Regime IV (HNLC, low dawn maximum) occurred upstream of the PF trough and eddy generation and south of the PF downstream of the trough. Regime I (higher dawn maximum) occurred on the equatorward side of the PF in the downstream transects. Based on our Fv/Fm data, this area is likely to have experienced higher dFe (Figure 4 and Figure S2 in Supporting Information S1).

4.3. pCO_2 Distribution and Ocean Carbon Uptake

Two parameters were used as the criteria to evaluate carbon uptake: (a) short term pCO_2 change at the same location and (b) organic carbon production estimated by the seasonal drawdown of nitrate. The strong increase in pCO_2 from south to north (Figure 8a) and the lower pCO_2 values on the return compared to outbound transect at the same latitude, can be attributed to biological drawdown by the large-scale bloom north of 51°S (Figures 1d, 1h, and 8). In the survey area, pCO_2 was maximum (>420 ppm) in the underway data between transects 6 and 7 and including the northern end of transect 6 and the southern half of transect 7 (Figure 8b). A week later, at the time of the strong bloom north and east of the front (Figure 3d), the ship revisited the location of the high pCO_2 and recorded values ∼40 ppm lower. This intense drawdown we attribute to the chlorophyll bloom. In week 3, at the time, transects 5–8 were made and chlorophyll was starting to increase, there was anticyclonic vorticity on the northern and eastern sides of the steepening trough (refer to Section 4.1.2; Figure S10 in Supporting Information S1). We speculate that the upwelled deep high DIC water caused the high pCO_2 section.

POC production was also estimated from nutrient drawdown between winter and the time of sampling, estimated as the difference between nutrients in the subsurface Antarctic Winter Water (T_{min}) layer and the sea surface. The primary productivity of the first five transects was low because the measurements occurred before the general increase in chlorophyll across the region. After transect 6, POC production increased, reaching about 35–40 μmol L^{-1} in the last two transects (Figure 8c). The rapid increase of POC production and biomass indicates a favorable environment that in this region of iron limitation suggests a possible input of dFe (Cassar et al., 2011; Moore et al., 2013; Viljoen et al., 2018). The magnitude of the productivity is close to that observed by Viljoen

et al. (2018) in an iron addition experiment in the Atlantic Antarctic zone (54–65°S), with a similar MLD to the downstream region in our study. Due to the different time scales of the POC calculation (through seasonal nitrate drawdown) and the in situ measurements, the patterns of POC production do not necessarily overlap with that of biomass.

4.4. Correlation Between MLD and Chlorophyll Biomass

We postulate that deep October MLDs enrich macronutrients and dFe in the surface and promote phytoplankton growth if the MLD shoals in November. This shoaling is quantified by a positive MLD_{diff} (Figure 9, upper panels). If the MLD_{diff} is near zero or negative (mixed layer deepening), this means that light limitation persists into November. Alternatively, and perhaps less likely, the mixed layer was already shallow in October, e.g., 2007, leading to relatively low phytoplankton biomass (Figure 9). We found that MLD_{diff} alone did not explain the interannual variability in chlorophyll. Some studies have raised questions about whether phytoplankton biomass increases monotonically with MLD shoaling. The "Dilution–Recoupling Hypothesis" suggests that a shallow MLD may increase the encounter rate between phytoplankton and predators, thus limiting the increase of phytoplankton (Behrenfeld, 2010; Evans & Parslow, 1985). The phytoplankton increase may also decline even before the MLD reaches the euphotic zone (Barber et al., 2001; Behrenfeld, 2010; Marra & Barber, 2005; Zhang et al., 2016). And even modest MLDs, by Southern Ocean standards, of about 50 m or deeper have been shown to induce light limitation of phytoplankton (Cassar et al., 2011; Eveleth et al., 2017).

The PF is part of the famous HNLC area, so interannual variability in dFe supply, e.g., through mesoscale structures, could play a key role in the variability of productivity. We hypothesize that a shoaling MLD (positive MLD_{diff}) with a shallow November MLD is a necessary condition for moderate productivity, allowing iron-rich waters to be entrained into the mixed layer. Strong cyclonic eddies or weak anticyclonic eddies, or both, also seem to be present when there is a strong bloom (Table S1 in Supporting Information S1). The eddy activity likely played multiple roles in both stimulating biomass and advecting it. This is supported by the overlay of eddy tracks on monthly mean SSH and chlorophyll (Figure S1 in Supporting Information S1). Cyclones are frequently found in the vicinity of high chlorophyll, e.g., in 2005 and 2018. When any of these factors changes or is absent, productivity is reduced. For example, in 2008 and 2009, negative MLD_{diff} (mixed layer deepening) could be the key to reduced productivity, while in 2012, anticyclonic eddy prevalence in November was implicated (Figure S1 and Table S1 in Supporting Information S1). Exceptions exist, however, like in 2014, where mixed layer shoaling (positive MLD_{diff}) and strong eddy activity would suggest high chlorophyll that did not eventuate (Table S1 in Supporting Information S1). The concentration of nutrients locally may be a factor in these cases. We suggest that future studies could more accurately define the relationship between the physical environment and productivity in such an energetic region of the ACC. This could be achieved by improving the observation system, through expanded coverage of biogeochemical Argo floats. We hope our study will accelerate such efforts.

5. Conclusion

This study provided a detailed description of biogeochemical variability around the standing meander of the PF in the Antarctic Circumpolar Current south of Tasmania. The unusually strong spring bloom in 2018 was potentially stimulated by the instability of the PF and the formation of mesoscale eddies. We quantified the distribution of macronutrients and biomass along the PF and divided the survey area into two physiological regimes according to the combination of dawn maximum and nocturnal decrease in Fv/Fm values. We theoretically inferred that the presence of the young cyclones and frontal processes along the PF may have promoted local upwelling, bringing macronutrients, and dFe to the surface. A mechanism such as this would support the unusually strong bloom observed in November 2018 and would account for the changed phytoplankton physiology, by increasing Fv/Fm, especially the dawn maximum. This was particularly visible in the north of the PF, downstream of the meander.

Increased consumption of DIC and production of POC were linked to a healthier phytoplankton community and increase in biomass. Through a remote sensing retrospective study from 2002 to 2019, we found a weak positive correlation between chlorophyll increase and MLD shoaling. However, intense blooms like that in 2018 likely require mesoscale structures and vertical motion to make nutrients and possibly iron available in the mixed layer. If the ACC becomes more energetic in the future, spawning more cyclonic eddies, this may stimulate Southern Ocean biogeochemical hotspots and strengthen the biological carbon pump. This study contributes to addressing

the research gap on the influence of mesoscale structures on Southern Ocean biogeochemical properties. Further progress in this area is important for understanding the changing landscape of primary productivity in a warming and more energetic Southern Ocean and its contribution to the climate system in the future.

Data Availability Statement

The shipboard data used in this study can be obtained from the CSIRO MNF at: https://www.marine.csiro.au/data/trawler/survey_details.cfm? survey= IN2018_V05 and the IMAS data portal via doi: 10.25959/Y5C2-Y445. The weekly surface chlorophyll data are available at NASA Goddard Space Flight Center via doi: 10.5067/JPSS1/VIIRS/L3M/CHL/2018, the SST for the same period are provided by the same mission via: https://oceancolor.gsfc.nasa.gov/data/viirs-j1/ and the chlorophyll climatologies are available at MODIS Aqua mission via doi: 10.5067/AQUA/MODIS/L3B/CHL/2018. Climatological nutrient data were obtained from NOAA's WOA18 at: https://accession.nodc.noaa.gov/NCEI-WOA18. SSH, wind speed, and geostrophic current velocity data were provided by Copernicus Marine Environment Monitoring Service (CMEMS) and the Copernicus Climate Change Service (C3S) at: https://duacs.cls.fr/duacs-products/. The full-depth temperature and salinity data were available at the International Argo Program and the national programs that contribute to it (http://www.argo.ucsd.edu, http://argo.jcommops.org). The Argo Program is part of the Global Ocean Observing System. The altimetric Mesoscale Eddy Trajectories Atlas product (META3.1exp DT allsat, doi: 10.24400/527896/a01-2021.001) was produced by SSALTO/DUACS and distributed by AVISO+ (https://www.aviso.altimetry.fr/) with support from CNES, in collaboration with IMEDEA. The sunrise Matlab toolbox is preserved at: https://github.com/beaudu/sunrise, the m_map mapping toolbox is preserved at: www.eos.ubc.ca/∼rich, and the Gibbs-SeaWater Oceanographic toolbox is preserved at: http://www.teos-10.org/index.htm.

Acknowledgments
This work was made possible through ship time on RV Investigator from Australia's Marine National Facility and funding from ARC Discovery Project DP170102162. We acknowledge the use of the CSIRO Marine National Facility—grid.473585.8—in undertaking this research. Xiang Yang, Pete Strutton, Nic Pitman, and Clara Vives thank the Australian Research Council Centre of Excellence for Climate Extremes (CE170100023) and the University of Tasmania for providing financial support to conduct the research. Helen Phillips acknowledges support from the Climate Systems Hub of the Australian government's National Environmental Science Programme. Nic Pittman and Clara Vives' participation in the voyage was also funded by the Australian Research Council's Special Research Initiative for Antarctic Gateway Partnership (Project ID SR140300001). Open access publishing facilitated by University of Tasmania, as part of the Wiley - University of Tasmania agreement via the Council of Australian University Librarians.

References

Abbott, M. R., Richman, J. G., Letelier, R. M., & Bartlett, J. S. (2000). The spring bloom in the Antarctic Polar Frontal Zone as observed from a mesoscale array of bio-optical sensors. *Deep Sea Research Part II: Topical Studies in Oceanography*, *47*, 3285–3314. https://doi.org/10.1016/S0967-0645(00)00069-2

Abbott, M. R., Richman, J. G., Nahorniak, J. S., & Barksdale, B. S. (2001). Meanders in the Antarctic Polar Frontal Zone and their impact on phytoplankton. *Deep Sea Research Part II: Topical Studies in Oceanography*, *48*, 3891–3912. https://doi.org/10.1016/S0967-0645(01)00073-X

Barber, R. T., Marra, J., Bidigare, R. C., Codispoti, L. A., Halpern, D., Johnson, Z., et al. (2001). Primary productivity and its regulation in the Arabian Sea during 1995. *Deep Sea Research Part II: Topical Studies in Oceanography*, *48*, 1127–1172. https://doi.org/10.1016/S0967-0645(00)00134-X

Barré, N., Provost, C., Renault, A., & Sennéchael, N. (2011). Fronts, meanders and eddies in Drake Passage during the ANT-XXIII/3 cruise in January-February 2006: A satellite perspective. *Deep Sea Research Part II: Topical Studies in Oceanography*, *58*, 2533–2554. https://doi.org/10.1016/j.dsr2.2011.01.003

Behrenfeld, M. J. (2010). Abandoning sverdrup's critical depth hypothesis on phytoplankton blooms. *Ecology*, *91*, 977–989. https://doi.org/10.1890/09-1207.1

Behrenfeld, M. J., Worthington, K., Sherrell, R. M., Chavez, F. P., Strutton, P., McPhaden, M., & Shea, D. M. (2006). Controls on tropical Pacific Ocean productivity revealed through nutrient stress diagnostics. *Nature*, *442*, 1025–1028. https://doi.org/10.1038/nature05083

Bindoff, N., & Phillips, H. (2019). *RV Investigator Voyage Scientific Highlights and Summary*.

Bischoff, T., & Thompson, A. F. (2014). Configuration of a Southern Ocean storm track. *Journal of Physical Oceanography*, *44*, 3072–3078. https://doi.org/10.1175/JPO-D-14-0062.1

Böning, C. W., Dispert, A., Visbeck, M., Rintoul, S. R., & Schwarzkopf, F. U. (2008). The response of the Antarctic Circumpolar Current to recent climate change. *Nature Geoscience*, *1*, 864–869. https://doi.org/10.1038/ngeo362

Bowie, A. R., Lannuzel, D., Remenyi, T. A., Wagener, T., Lam, P. J., Boyd, P. W., et al. (2009). Biogeochemical iron budgets of the Southern Ocean south of Australia: Decoupling of iron and nutrient cycles in the subantarctic zone by the summertime supply. *Global Biogeochemical Cycles*, *23*, GB4034. https://doi.org/10.1029/2009GB003500

Boyd, P. W., & Abraham, E. R. (2001). Iron-mediated changes in phytoplankton photosynthetic competence during SOIREE. *Deep Sea Research Part II: Topical Studies in Oceanography*, *48*, 2529–2550. https://doi.org/10.1016/S0967-0645(01)00007-8

Boyd, P. W., & Law, C. S. (2001). The Southern Ocean Iron RElease Experiment (SOIREE)—Introduction and summary. *Deep Sea Research Part II: Topical Studies in Oceanography*, *48*, 2425–2438. https://doi.org/10.1016/S0967-0645(01)00002-9

Cassar, N., Difiore, P. J., Barnett, B. A., Bender, M. L., Bowie, A. R., Tilbrook, B., et al. (2011). The influence of iron and light on net community production in the Subantarctic and Polar Frontal Zones. *Biogeosciences*, *8*, 227–237. https://doi.org/10.5194/bg-8-227-2011

Cavalieri, D. J., Parkinson, C. L., Gloersen, P., & Zwally, H. J. (1996). Sea ice concentrations from Nimbus-7 SMMR and DMSP SSM/I passive micro-wave data. National Snow and Ice Data Center (updated 2021). Retrieved from http://nsidc.org/data/nsidc-0051.html

Chapman, C. C., Hogg, A. M. C., Kiss, A. E., & Rintoul, S. R. (2015). The dynamics of Southern Ocean storm tracks. *Journal of Physical Oceanography*, *45*, 884–903. https://doi.org/10.1175/JPO-D-14-0075.1

de Baar, H., Buma, A., Nolting, R., Cadee, G., Jacques, G., & Treguer, P. (1990). On iron limitation of the Southern Ocean: Experimental observations in the Weddell and Scotia Seas. *Marine Ecology Progress Series*, *65*, 105–122. https://doi.org/10.3354/meps065105

Della-Penna, A., Trull, T. W., Wotherspoon, S., De Monte, S., Johnson, C. R., & D'Ovidio, F. (2018). Mesoscale variability of conditions favoring an iron-induced diatom bloom downstream of the Kerguelen Plateau. *Journal of Geophysical Research: Oceans*, *123*, 3355–3367. https://doi.org/10.1029/2018JC013884

Dong, C., Nencioli, F., Liu, Y., & McWilliams, J. C. (2011). An automated approach to detect oceanic eddies from satellite remotely sensed sea surface temperature data. *IEEE Geoscience and Remote Sensing Letters*, *8*, 1055–1059. https://doi.org/10.1109/LGRS.2011.2155029

Du, Y., Song, W., He, Q., Huang, D., Liotta, A., & Su, C. (2019). Deep learning with multi-scale feature fusion in remote sensing for automatic oceanic eddy detection. *Information Fusion*, *49*, 89–99. https://doi.org/10.1016/j.inffus.2018.09.006

Ellwood, M. J., Boyd, P. W., & Sutton, P. (2008). Winter-time dissolved iron and nutrient distributions in the Subantarctic Zone from 40-52S; 155-160E. *Geophysical Research Letters*, *35*, L11604. https://doi.org/10.1029/2008GL033699

Evans, G. T., & Parslow, J. S. (1985). A model of annual plankton cycles. *Biological Oceanography*, *32*, 327–347. https://doi.org/10.1016/0198-0254(85)92902-4

Eveleth, R., Cassar, N., Sherrell, R. M., Ducklow, H., Meredith, M. P., Venables, H. J., et al. (2017). Ice melt influence on summertime net community production along the Western Antarctic Peninsula. *Deep Sea Research Part II: Topical Studies in Oceanography*, *139*, 89–102. https://doi.org/10.1016/j.dsr2.2016.07.016

Fisher, T. R., Peele, E. R., Ammerman, J. W., & Harding, L. W. (1992). Nutrient limitation of phytoplankton in Chesapeake Bay. *Marine Ecology Progress Series*, *82*, 51–63. https://doi.org/10.3354/meps082051

Freeman, N. M., Munro, D. R., Sprintall, J., Mazloff, M. R., Purkey, S., Rosso, I., et al. (2019). The observed seasonal cycle of macronutrients in Drake Passage: Relationship to fronts and utility as a model metric. *Journal of Geophysical Research: Oceans*, *124*, 4763–4783. https://doi.org/10.1029/2019JC015052

Frenger, I., Munnich, M., Gruber, N., & Knutti, R. (2015). Southern Ocean eddy phenomenology. *Journal of Geophysical Research: Oceans*, *120*, 7413–7449. https://doi.org/10.1002/2015JC011047

Garabato, A. C. N., Allen, A. T., Leach, H., Strass, V. H., & Pollard, R. T. (2001). Mesoscale subduction at the Antarctic Polar Front driven by baroclinic instability. *Journal of Physical Oceanography*, *31*, 2087–2107. https://doi.org/10.1175/1520-0485(2001)031<2087:msatap>2.0.co;2;2

Gaube, P., Chelton, D. B., Samelson, R. M., Schlax, M. G., & O'Neill, L. W. (2015). Satellite observations of mesoscale eddy-induced Ekman pumping. *Journal of Physical Oceanography*, *45*, 104–132. https://doi.org/10.1175/JPO-D-14-0032.1

Gaube, P., Chelton, D. B., Strutton, P. G., & Behrenfeld, M. J. (2013). Satellite observations of chlorophyll, phytoplankton biomass, and Ekman pumping in nonlinear mesoscale eddies. *Journal of Geophysical Research: Oceans*, *118*, 6349–6370. https://doi.org/10.1002/2013JC009027

Gaube, P. Jr., McGillicuddy, D. J., Chelton, D. B., Behrenfeld, M. J., & Strutton, P. G. (2014). Regional variations in the influence of mesoscale eddies on near-surface chlorophyll. *Journal of Geophysical Research: Oceans*, *119*, 8195–8220. https://doi.org/10.1002/2014JC010111

Grenier, M., Della Penna, A., & Trull, T. W. (2015). Autonomous profiling float observations of the high-biomass plume downstream of the Kerguelen Plateau in the Southern Ocean. *Biogeosciences*, *12*, 2707–2735. https://doi.org/10.5194/bg-12-2707-2015

Hallberg, R., & Gnanadesikan, A. (2006). The role of eddies in determining the structure and response of the wind-driven southern hemisphere overturning: Results from the modeling eddies in the Southern Ocean (MESO) Project. *Journal of Physical Oceanography*, *36*, 2232–2252. https://doi.org/10.1175/JPO2980.1

Hoffmann, L. J., Peeken, I., & Lochte, K. (2008). Iron, silicate, and light co-limitation of three Southern Ocean diatom species. *Polar Biology*, *31*, 1067–1080. https://doi.org/10.1007/s00300-008-0448-6

Hughes, P., Janssens, J., Rayner, M., & Frampton, D. (2018). RV Investigator hydrochemistry data processing report.

Janssen, D. J., Sieber, M., Ellwood, M. J., Conway, T. M., Barrett, P. M., Chen, X., et al. (2020). Trace metal and nutrient dynamics across broad biogeochemical gradients in the Indian and Pacific sectors of the Southern Ocean. *Marine Chemistry*, *221*, 103773. https://doi.org/10.1016/j.marchem.2020.103773

Jennings, J. C., Gordon, L. I., & Nelson, D. M. (1984). Nutrient depletion indicates high primary productivity in the Weddell Sea. *Nature*, *309*(1950), 51–54. https://doi.org/10.1038/309051a0

Jones, E. M., Hoppema, M., Strass, V., Hauck, J., Salt, L., Ossebaar, S., et al. (2015). Mesoscale features create hotspots of carbon uptake in the Antarctic Circumpolar Current. *Deep Sea Research Part II: Topical Studies in Oceanography*, *138*, 39–51. https://doi.org/10.1016/j.dsr2.2015.10.006

Kahru, M., Mitchell, B. G., Gille, S. T., Hewes, C. D., & Holm-Hansen, O. (2007). Eddies enhance biological production in the Weddell-Scotia confluence of the Southern Ocean. *Geophysical Research Letters*, *34*, L14603. https://doi.org/10.1029/2007GL030430

Landschützer, P., Gruber, N., Haumann, A., Rödenbeck, C., Bakker, D. C. E., van Heuven, S., et al. (2015). The reinvigoration of the Southern Ocean carbon sink. *Science*, *349*, 1221–1224. https://doi.org/10.1126/science.aab2620

Lannuzel, D., Bowie, A. R., Remenyi, T., Lam, P., Townsend, A., Ibisanmi, E., et al. (2011). Distributions of dissolved and particulate iron in the sub-Antarctic and Polar Frontal Southern Ocean (Australian sector). *Deep Sea Research Part II: Topical Studies in Oceanography*, *58*, 2094–2112. https://doi.org/10.1016/j.dsr2.2011.05.027

Le Quéré, C., Andrew, R. M., Friedlingstein, P., Sitch, S., Pongratz, J., Manning, A. C., et al. (2018). Global carbon budget 2018 (pre-print). *Earth System Science Data Discussions*, 1–54. https://doi.org/10.5194/essd-2017-123

Lévy, M., Ferrari, R., Franks, P. J. S., Martin, A. P., & Rivière, P. (2012). Bringing physics to life at the submesoscale. *Geophysical Research Letters*, *39*, L14602. https://doi.org/10.1029/2012GL052756

Lévy, M., Klein, P., & Treguier, A. M. (2001). Impact of sub-mesoscale physics on production and subduction of phytoplankton in an oligotrophic regime. *Journal of Marine Research*, *59*, 535–565. https://doi.org/10.1357/002224001762842181

Lindstrom, S. S., Qian, X., & Randolph, D. (1997). Vertical motion in the Gulf Stream and its relation to meanders. *Journal of Geophysical Research*, *102*, 8485–8503. https://doi.org/10.1029/96JC03498

Mahadevan, A., Thomas, L. N., & Tandon, A. (2008). Comment on "Eddy/wind interactions stimulate extraordinary mid-ocean plankton blooms". *Science*, *80*, 320–448. https://doi.org/10.1126/science.1152111

Marra, J., & Barber, R. T. (2005). Primary productivity in the Arabian Sea: A synthesis of JGOFS data. *Progress in Oceanography*, *65*, 159–175. https://doi.org/10.1016/j.pocean.2005.03.004

Marshall, D. P., Ambaum, M. H. P., Maddison, J. R., Munday, D. R., & Novak, L. (2017). Eddy saturation and frictional control of the Antarctic Circumpolar Current. *Geophysical Research Letters*, *44*, 286–292. https://doi.org/10.1002/2016GL071702

Martin, A. P., & Richards, K. J. (2001). Mechanisms for vertical nutrient transport within a North Atlantic mesoscale eddy. *Deep Sea Research Part II: Topical Studies in Oceanography*, *48*, 757–773. https://doi.org/10.1016/S0967-0645(00)00096-5

McDougall, T. J., & Barker, P. M. (2011). *Getting started with TEOS-10 and the Gibbs Seawater (GSW), Scor/Iapso Wg127*.

McGillicuddy, D. J. (2016). Mechanisms of physical-biological-biogeochemical interaction at the oceanic mesoscale. *Annual Review of Marine Science*, *8*, 125–159. https://doi.org/10.1146/annurev-marine-010814-015606

McGillicuddy, D. J., Robinson, A. R., Siegel, D. A., Jannasch, H. W., Johnsonk, R., Dickey, T. D., et al. (1998). Influence of mesoscale eddies on new production in the Sargasso Sea. *Nature*, *394*, 263–266. https://doi.org/10.1038/28367

Meijer, J. J., Phillips, H. E., Bindoff, N. L., Rintoul, S. R., & Foppert, A. (2022). Dynamics of a standing meander of the subantarctic front diagnosed from satellite altimetry and along-stream anomalies of temperature and salinity. *Journal of Physical Oceanography*, *52*, 1073–1089. https://doi.org/10.1175/JPO-D-21-0049.1

Meredith, M. P., & Hogg, A. M. (2006). Circumpolar response of Southern Ocean eddy activity to a change in the Southern Annular Mode. *Geophysical Research Letters*, *33*, L16608. https://doi.org/10.1029/2006GL026499

Moore, C. M., Mills, M. M., Arrigo, K. R., Berman-Frank, I., Bopp, L., Boyd, P. W., et al. (2013). Processes and patterns of oceanic nutrient limitation. *Nature Geoscience*, *6*, 701–710. https://doi.org/10.1038/ngeo1765

Moreau, S., Penna, A. D., Llort, J., Patel, R., Langlais, C., Boyd, P. W., et al. (2017). Eddy-induced carbon transport across the Antarctic Circumpolar Current. *Global Biogeochemical Cycles*, *31*, 1368–1386. https://doi.org/10.1002/2017GB005669

Morel, A., & Maritorena, S. (2001). Bio-optical properties of oceanic waters: A reappraisal. *Journal of Geophysical Research*, *106*, 7163–7180. https://doi.org/10.1029/2000JC000319

Munday, D. R., Johnson, H. L., & Marshall, D. P. (2013). Eddy saturation of equilibrated circumpolar currents. *Journal of Physical Oceanography*, *43*, 507–532. https://doi.org/10.1175/JPO-D-12-095.1

Orsi, A. H., Whitworth, T., & Nowlin, W. D. (1995). On the meridional extent and fronts of the Antarctic Circumpolar Current. *Deep Sea Research Part I*, *42*, 641–673. https://doi.org/10.1016/0967-0637(95)00021-W

Patel, R. S., Llort, J., Strutton, P. G., Phillips, H. E., Moreau, S., Conde Pardo, P., & Lenton, A. (2020). The biogeochemical structure of Southern Ocean mesoscale eddies. *Journal of Geophysical Research: Oceans*, *125*, e2020JC016115. https://doi.org/10.1029/2020JC016115

Patel, R. S., Phillips, H. E., Strutton, P. G., Lenton, A., & Llort, J. (2019). Meridional heat and salt transport across the subantarctic front by cold-core eddies. *Journal of Geophysical Research: Oceans*, *124*, 981–1004. https://doi.org/10.1029/2018JC014655

Phillips, H. E., & Rintoul, S. R. (2000). Eddy variability and energetics from direct current measurements in the Antarctic Circumpolar Current south of Australia. *Journal of Physical Oceanography*, *30*, 3050–3076. https://doi.org/10.1175/1520-0485(2000)030<3050:evaefd>2.0.co;2;2

Rees, C., Pender, L., Sherrin, K., Schwanger, C., Hughes, P., Tibben, S., et al. (2019). Methods for reproducible shipboard SFA nutrient measurement using RMNS and automated data processing. *Limnology and Oceanography: Methods*, *17*, 25–41. https://doi.org/10.1002/lom3.10294

Ries, J. B., Cohen, A. L., & McCorkle, D. C. (2009). Marine calcifiers exhibit mixed responses to CO_2-induced ocean acidification. *Geology*, *37*, 1131–1134. https://doi.org/10.1130/G30210A.1

Rintoul, S. R. (2018). The global influence of localized dynamics in the Southern Ocean. *Nature*, *558*, 209–218. https://doi.org/10.1038/s41586-018-0182-3

Rintoul, S. R., & Naveira Garabato, A. C. (2013). Dynamics of the Southern Ocean circulation. In *International geophysics* (pp. 471–492). Elsevier Ltd. https://doi.org/10.1016/B978-0-12-391851-2.00018-0

Rodríguez, J., Tintoré, J., Allen, J. T., Blanco, J. M., Gomis, D., Reul, A., et al. (2001). Mesoscale vertical motion and the size structure of phytoplankton in the ocean. *Nature*, *410*, 360–363. https://doi.org/10.1038/35066560

Roemmich, D., & Gilson, J. (2009). The 2004-2008 mean and annual cycle of temperature, salinity, and steric height in the global ocean from the Argo Program. *Progress in Oceanography*, *82*, 81–100. https://doi.org/10.1016/j.pocean.2009.03.004

Sabine, C. L., Feely, R. A., Gruber, N., Key, R. M., Lee, K., Bullister, J. L., et al. (2004). The oceanic sink for anthropogenic CO_2. *Science*, *305*, 367–371. https://doi.org/10.1126/science.1097403

Sarmiento, J. L., & Gruber, N. (2006). Ocean biogeochemical dynamics. In *Encyclopedia of Earth sciences series* (pp. 983–986). https://doi.org/10.1515/9781400849079check doi

Schlitzer, R. (2002). Carbon export fluxes in the Southern Ocean: Results from inverse modeling and comparison with satellite-based estimates. *Deep Sea Research Part II: Topical Studies in Oceanography*, *49*, 1623–1644. https://doi.org/10.1016/S0967-0645(02)00004-8

Sokolov, S., & Rintoul, S. R. (2009). Circumpolar structure and distribution of the Antarctic Circumpolar Current fronts: 1. Mean circumpolar paths. *Journal of Geophysical Research*, *114*, C11018. https://doi.org/10.1029/2008JC005108

Song, H., Marshall, J., Munro, D. R., Dutkiewicz, S., Sweeney, C. Jr., McGillicuddy, D. J., & Hausmann, U. (2016). Mesoscale modulation of air-sea CO_2 flux in Drake Passage. *Journal of Geophysical Research: Oceans*, *121*, 6635–6649. https://doi.org/10.1002/2016JC011714

Strass, V. H. (1992). Chlorophyll patchiness caused by mesoscale upwelling at fronts. *Deep Sea Research Part I: Oceanographic Research Papers*, *39*, 75–96. https://doi.org/10.1016/0198-0149(92)90021-K

Strutton, P. G., Chavez, F. P., Dugdale, R. C., & Hogue, V. (2004). Primary productivity in the central equatorial Pacific (3°S 130°W) during GasEx-2001. *Journal of Geophysical Research*, *109*, C08S06. https://doi.org/10.1029/2003JC001790

Su, J., Strutton, P. G., & Schallenberg, C. (2021). The subsurface biological structure of Southern Ocean eddies revealed by BGC-Argo floats. *Journal of Marine Systems*, *220*, 103569. https://doi.org/10.1016/j.jmarsys.2021.103569

Talley, L. D., Pickard, G. L., Emery, W. J., & H, J. S. (2011). *Descriptive physical oceanography: An introduction* (6th ed.). Elsevier. https://doi.org/10.16309/j.cnki.issn.1007-1776.2003.03.004

Tamsitt, V., Drake, H. F., Morrison, A. K., Talley, L. D., Dufour, C. O., Gray, A. R., et al. (2017). Spiraling pathways of global deep waters to the surface of the Southern Ocean. *Nature Communications*, *8*, 172. https://doi.org/10.1038/s41467-017-00197-0

Tang, W., Llort, J., Weis, J., Perron, M. M. G., Basart, S., Li, Z., et al. (2021). Widespread phytoplankton blooms triggered by 2019–2020 Australian wildfires. *Nature*, *597*, 370–375. https://doi.org/10.1038/s41586-021-03805-8

Thompson, A. F., & Garabato, A. C. N. (2014). Equilibration of the Antarctic Circumpolar Current by standing meanders. *Journal of Physical Oceanography*, *44*, 1811–1828. https://doi.org/10.1175/JPO-D-13-0163.1

Viljoen, J. J., Philibert, R., Van Horsten, N., Mtshali, T., Roychoudhury, A. N., Thomalla, S., & Fietz, S. (2018). Phytoplankton response in growth, photophysiology and community structure to iron and light in the Polar Frontal Zone and Antarctic waters. *Deep Sea Research Part I: Oceanographic Research Papers*, *141*, 118–129. https://doi.org/10.1016/j.dsr.2018.09.006

Wang, K. (2020). *Characterising upwelling of Circumpolar Deep Water at the Polar Front and investigating submesoscale processes associated with upwelling*. Honours thesis. (p. 71). University of Tasmania.

Watts, D. R., Tracey, K. L., Donohue, K. A., & Chereskin, T. K. (2016). Estimates of eddy heat flux crossing the Antarctic Circumpolar Current from observations in drake passage. *Journal of Physical Oceanography*, *46*, 2103–2122. https://doi.org/10.1175/JPO-D-16-0029.1

Williams, R. G., Wilson, C., & Hughes, C. W. (2007). Ocean and atmosphere storm tracks: The role of eddy vorticity forcing. *Journal of Physical Oceanography*, *37*, 2267–2289. https://doi.org/10.1175/JPO3120.1

Wolfe, K., & Byrne, M. (2016). *Ocean acidification is already harming the Great Barrier Reef's growth* [WWW Document]. Conversat.

Zhang, C. H., Xi, X. L., Liu, S. T., Shao, L. J., & Hu, X. H. (2014). A mesoscale eddy detection method of specific intensity and scale from SSH image in the South China Sea and the Northwest Pacific. *Science China Earth Sciences*, *57*(1897), 1906. https://doi.org/10.1007/s11430-014-4839-y

Zhang, R., Xie, S. P., Xu, L., & Liu, Q. (2016). Changes in mixed layer depth and spring bloom in the Kuroshio extension under global warming. *Advances in Atmospheric Sciences*, *33*, 452–461. https://doi.org/10.1007/s00376-015-5113-8